Complementary Ca2+ Activity of Sensory Activated and Suppressed Layer 6 Corticothalamic Neurons Reflects Behavioral State

Article

Current Biology

Complementary Ca^{2+} Activity of Sensory Activated and Suppressed Layer 6 Corticothalamic Neurons Reflects Behavioral State

Highlights

- V1 layer 6 corticothalamic neurons were imaged during different behavioral states
- L6CT neurons are either visual stimulus activated (VSA), suppressed (VSS), or quiet
- Activity of VSA and VSS neurons complement each other to a constant level
- Complementary VSA and VSS neuron activity level is behavioral state dependent

Authors

Sigita Augustinaite, Bernd Kuhn

Correspondence

sigita.augustinaite@oist.jp (S.A.), bkuhn@oist.jp (B.K.)

In Brief

Augustinaite and Kuhn image the deepest cortical layer, layer 6, in mice with two-photon microscopy. In visual cortex, layer 6 corticothalamic neurons are either visual stimulus activated, suppressed, or quiet. Interestingly, the Ca^{2+} activity of these neuronal populations complements each other and generates a constant activity level that is behavioral state dependent.

Augustinaite & Kuhn, 2020, Current Biology *30*, 1–16
October 19, 2020
https://doi.org/10.1016/j.cub.2020.07.069

CellPress

Please cite this article in press as: Augustinaite and Kuhn, Complementary Ca^{2+} Activity of Sensory Activated and Suppressed Layer 6 Corticothalamic Neurons Reflects Behavioral State, Current Biology (2020), https://doi.org/10.1016/j.cub.2020.07.069

Current Biology

CellPress
OPEN ACCESS

Article

Complementary Ca^{2+} Activity of Sensory Activated and Suppressed Layer 6 Corticothalamic Neurons Reflects Behavioral State

Sigita Augustinaite[1,*] and Bernd Kuhn[1,2,*]
[1]Optical Neuroimaging Unit, Okinawa Institute of Science and Technology Graduate University, 1919-1 Tancha, Onna-son, 904-0495 Okinawa, Japan
[2]Lead Contact
*Correspondence: sigita.augustinaite@oist.jp (S.A.), bkuhn@oist.jp (B.K.)
https://doi.org/10.1016/j.cub.2020.07.069

SUMMARY

Layer 6 (L6) corticothalamic neurons project to thalamus, where they are thought to regulate sensory information transmission to cortex. However, the activity of these neurons during different behavioral states has not been described. Here, we imaged calcium changes in visual cortex L6 primary corticothalamic neurons with two-photon microscopy in head-fixed mice in response to passive viewing during a range of behavioral states, from locomotion to sleep. In addition to a substantial fraction of quiet neurons, we found sensory-activated and suppressed neurons, comprising two functionally distinct L6 feedback channels. Quiet neurons could be dynamically recruited to one or another functional channel, and the opposite, functional neurons could become quiet under different stimulation conditions or behavior states. The state dependence of neuronal activity was heterogeneous with respect to locomotion or level of alertness, although the average activity was largest during highest vigilance within populations of functional neurons. Interestingly, complementary activity of these distinct populations kept the overall corticothalamic feedback relatively constant during any given behavioral state. Thereby, in addition to sensory and non-sensory information, a constant activity level characteristic of behavioral state is conveyed to thalamus, where it can regulate signal transmission from the periphery to cortex.

INTRODUCTION

Cortical layer 6 (L6) is arguably the most enigmatic lamina of cortex. It comprises different populations of excitatory neurons with distinct morphology, inputs, and projection targets, which enable them to participate in different circuits [1, 2]. The most numerous sub-class of primary cortex L6 pyramidals are corticothalamic neurons (CTs), which send topologically arranged and massive projections to thalamus [3, 4].

This corticothalamic feedback is considered to be one of the key players in brain-state-dependent regulation of sensory signal transmission through thalamocortical neurons (TCs) [5–8]. It affects the spatiotemporal structure of the receptive fields [9–11], response mode (burst or tonic), gain, and reliability of the responses of TC neurons to sensory stimulation [12–15] through dynamic interplay of excitation and di-synaptic inhibition via intrinsic interneurons or thalamic reticular nucleus [16–19]. However, very little is known about the activity of L6CTs, especially during different behavioral states and cognitive processes, due to complex cortical connectivity [1–4, 20], the highly intricate and dynamic thalamocortical network activity [8, 21, 22], and regulation of this network by neuromodulators [7, 23, 24].

Visual cortex (V1) L6 primary corticothalamic neurons are involved in regulation of sensory signal transmission from retina to V1 via the dorsal lateral geniculate nucleus (dLGN). These CTs fall into four transcriptional profiles with similar electrophysiological features [25] and two morphological categories: neurons with short apical dendrites and tufts in L4 and neurons with long apical dendrites with branches in L4 and tufts in L1 [25, 26]. Through the basal dendrites in L6 as well as apical tufts in L4 and L1, the CTs receive bottom-up inputs from thalamus [27–30], which carry sensory as well as behavioral state and context information [31–33]. Dendrites in superficial and deep layers integrate state-dependent [34–38] local and long-range cortico-cortical inputs [1, 2, 39–42]. These inputs are involved in control of gain and various aspects of cognition, including attention, expectation, or memory [43–47], and reflect the instantaneous state of the network or the internal model of the surrounding world [48–50].

Thus, CTs should continuously integrate external sensory drive with motor and higher cognitive information in the context of behavior and the sleep/wake cycle and send this information down to thalamus. However, it is not clear how this diverse information is integrated. Importantly, it is not even known to what extent corticothalamic feedback is related to behavioral state or sensory signal processing.

Here, we performed 1 to 3 h of continuous two-photon (2P) calcium imaging of V1 L6 in spontaneously behaving, head-fixed Ntsr1-Cre mice [51] during different levels of alertness, ranging from high vigilance to sleep. Soma activity of dLGN-projecting

Please cite this article in press as: Augustinaite and Kuhn, Complementary Ca^{2+} Activity of Sensory Activated and Suppressed Layer 6 Corticothalamic Neurons Reflects Behavioral State, Current Biology (2020), https://doi.org/10.1016/j.cub.2020.07.069

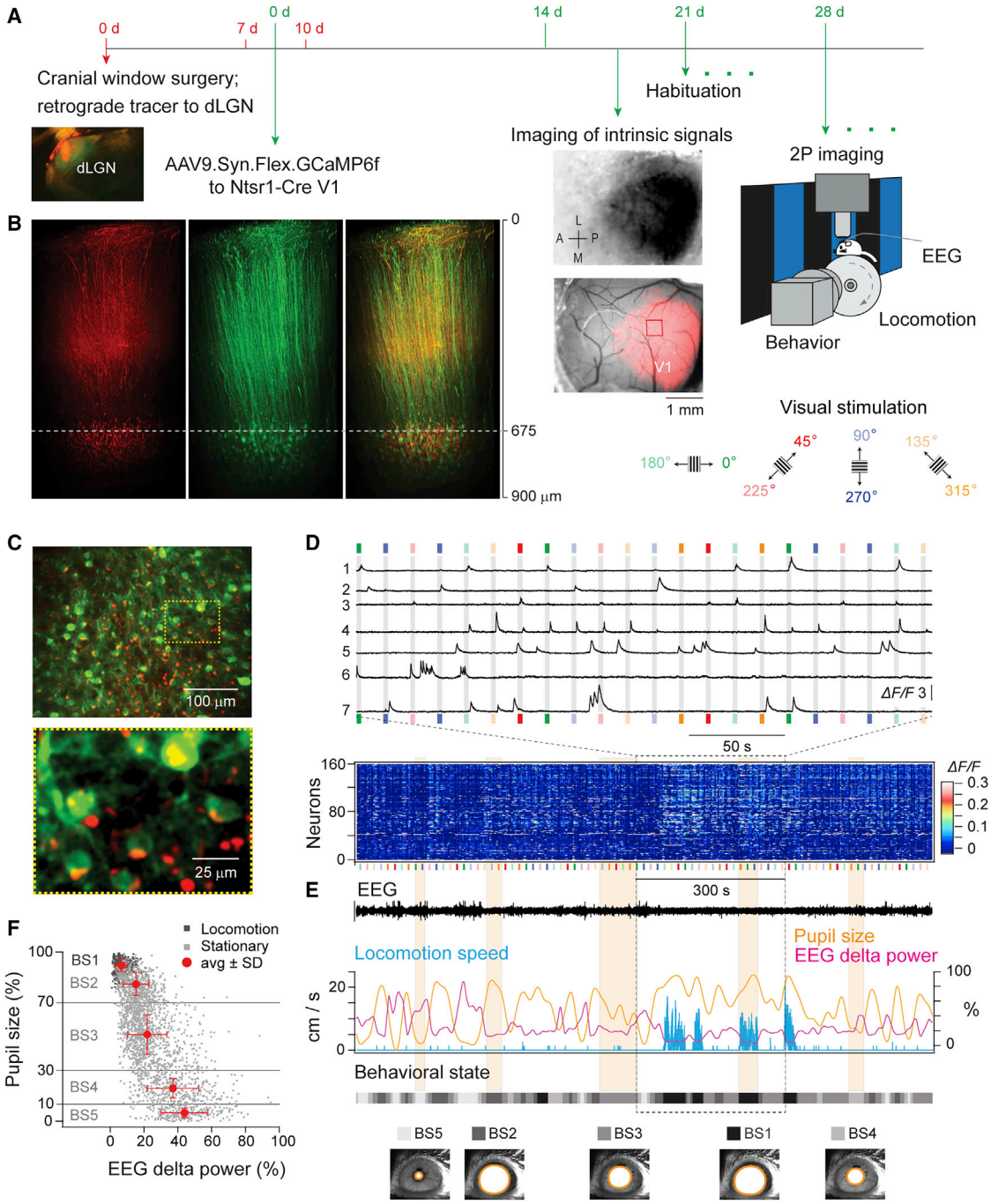

Figure 1. 2P Imaging of Activity of Primary Visual Cortex L6 Corticothalamic Neurons in Head-Fixed Spontaneously Behaving Mouse

(A) Sequence of experimental procedures: retrograde tracer (red) injection into dLGN and mounting of chronic cranial window with access port; AAV injection for GCaMP6f expression in CT neurons; imaging of intrinsic signals to map V1 and target imaging site (top, activated area indicating V1; bottom, brain surface blood vessel pattern superimposed with area of V1 and imaging site); and schematic drawing of two-photon calcium imaging in a head-fixed behaving mouse while presenting 8 directions of full-screen drifting gratings as visual stimuli (Δ 45°, 2 Hz temporal, and 0.08 cycles/deg spatial frequency).

(B) 2P reconstruction of the imaging site shown in (A). Left: axons of TC neurons (labeled by AAV injection for TurboRFP expression in dLGN) and retrogradely transported beads in the somata of L6CT neurons (both red) are shown. Middle: L6CT neurons selectively labeled with GCaMP6f (green) are shown. Right: overlay shows overlap of axonal projections and dendritic density throughout the cortex and overlap of beads and CT somata in L6. See also Video S1.

(C) Crop of imaging plane indicated by dotted line in (B) shows CT neurons (green) and beads (red); enlarged image (bottom).

(D) Neuronal calcium activity (Δ*F*/*F*) of dLGN projecting L6CT neurons in a behaving mouse. Individual neurons (top) and population activity of all selected CT neurons (n = 159, single imaging site; bottom) show sparse activity. Some neurons (traces 1–4) respond to visual stimuli (direction defined by color code in A), although others do not (traces 5–7). See also Figure S1.

(legend continued on next page)

Please cite this article in press as: Augustinaite and Kuhn, Complementary Ca^{2+} Activity of Sensory Activated and Suppressed Layer 6 Corticothalamic Neurons Reflects Behavioral State, Current Biology (2020), https://doi.org/10.1016/j.cub.2020.07.069

CTs in response to passive viewing of periodically presented full-screen drifting gratings was recorded while monitoring behavior state parameters: locomotion speed; electroencephalogram (EEG); and pupil diameter. The morphology of these neurons was correlated with functional imaging data by using dendritic reconstructions of representative CTs. This allowed us to characterize the dynamic population activity of L6CTs with single-cell resolution and to describe the behavioral state-related feedback sent to primary thalamus.

RESULTS

Two-Photon Calcium Imaging of V1 L6CT Neurons Projecting to dLGN in Behaving Mice

The experiment involved several procedures (Figure 1A). During the chronic cranial window installation surgery, the retrograde-tracing fluorescent microspheres were injected into dLGN to identify V1 L6CTs projecting to primary thalamus. AAV9-CAG-Flex-GCaMP6f was injected through the access port [52] 1 to 2 weeks post-surgery to co-label the cortical site with retrograde beads. The area of V1 was confirmed by imaging of intrinsic signals [53]. 2P calcium imaging was performed in setup-habituated mice, which were head fixed on a cylindrical treadmill during the passive viewing of visual stimuli (8 directions full screen drifting gratings). To track the behavioral state of the animal, we recorded the EEG, the locomotion speed, and a behavior movie for information about pupil size and whisking or grooming periods.

In some animals, AAV1-hSYN-TurboRFP was co-injected with the beads into dLGN to label thalamocortical projections (red, Figure 1B; Video S1). L6CTs could be reconstructed down to 800–900 μm below dura (green, Figure 1B; Video S1). The core functional imaging dataset was collected from upper L6 (e.g., 675 μm; Figures 1B, 1C, S1A, and S1B). Projections and the retrograde transport of beads to the same cortical area confirmed the topologically conserved thalamocortical loop (composite; Figure 1B; Video S1). Only CTs projecting to dLGN (neurons with both GCaMP6f expression and retrograde beads) were examined in the core experiments of this study (about 60% of GCaMP6f expressing neurons; n = 485, 3 mice; Figure 1C).

Clear chronic cranial windows and GCaMP6f expression limited to L6 pyramidal neurons were essential to image at high contrast close to the fundamental imaging depth limit of 2P microscopy [54] (Figure S1). Additionally, the point spread function of excitation was extended to 5 μm in z direction by under-filling the objective back aperture [55] and by adjusting the objective collar to maximal imaging depth [56]. The under-filling increased the fluorescence intensity and minimized photo-damage because of the increased excitation volume. These adjustments allowed imaging of the same L6 neurons continuously for 1–3 h per day, for several (2–4) days, to collect the data under various levels of alertness.

CTs showed sparse and heterogeneous activity patterns (Figures 1D and S1E), but only some of them were driven by the visual stimuli (e.g., Figures 1D [traces 1–4] and S1E [traces 1, 2, or 14]). Population activity was stronger during more active or alert states, indicated by locomotion, large pre-stimulus pupil size, and low EEG delta power (Figures 1D and 1E; Videos S2 and S3; see below for details).

Moving versus stationary behavior states are well-established indicators of the alertness in the mouse visual system [31, 36, 37, 57, 58]. Also, the pupil size was acknowledged as a reliable measure of state even during stationary periods, covering the different regimes of alertness and sleep [34, 35, 59–61]. As in other studies [34, 35, 59, 60], the pupil size continuously varied in negative correlation with cortical synchrony level (EEG delta power), but no discrete steps were observed (Figure 1F). Therefore, we defined 5 behavioral states (BSs) based on locomotion and exposed pre-stimulus pupil area ("pupil size", unless stated otherwise; Figures 1E and 1F): locomotion state BS1 and stationary states from BS2 (the most alert state with the same pupil size as during BS1 [>70%]) to BS5 (non-REM sleep with the smallest pupil size [≤10%]). REM sleep periods, if occurring, always following BS5 (data not shown) were removed from the analysis.

Visual Stimulus Activated, Suppressed, and Quiet L6CT Neurons

To characterize the activity of individual neurons during different conditions defined by behavioral state and visual stimulus direction, an activity matrix was generated by averaging all trials of a particular state and stimulus (Figures 2A and 2B). Then, the maximum response (Rmax) for every neuron was determined, which is the largest average change (positive or negative) in $\Delta F/F$ elicited during one of the five behavioral states by one of the eight visual stimuli (BS2, 90° and BS1, 135°; Figures 2A and 2B). Based on the sign of the maximum response, neurons were defined either as visual stimulus activated (VSA) (Rmax > 0) or visual stimulus suppressed (VSS) (Rmax < 0; Figures 2C and 2D). However, the calcium activity of 39% of all neurons was very low (average $\Delta F/F < 10\%$ during 4 s after the onset of the stimulus for VSAs or 4 s before for VSSs in all trials). These neurons were defined as Quiet (gray, n = 188 of 485; Figure 2C). Only active neurons (VSA, 32%, n = 158, red; VSS, 29%, n = 139, blue; Figure 2C) were used further, unless indicated otherwise.

The highest activity of VSAs was triggered by the onset or offset of the visual stimuli, although spontaneous activity, typically, was low (Figures 2A, 2C, and 2D). The activity of VSSs, on the contrary, was highest during the dark periods and was reliably suppressed with the onset of visual stimuli (Figures 2B–2D). Typically, the response type (VSA or VSS) did not

(E) Monitoring of behavioral state: EEG trace (0.25–100 Hz), EEG delta power (0.5–4 Hz, magenta), locomotion speed (blue), normalized pre-stimulus pupil size (orange), and time course of behavior states (gray scale), defined by the pre-stimulus pupil size (bottom: example images of an eye for the 5 different states; corresponding state periods marked by the vertical light orange highlights). See also Videos S2 and S3.

(F) Scatterplot of normalized pre-stimulus pupil size versus delta power used for the definition of the behavioral state (each dot indicates the behavioral state during a single 12-s trial, including one visual stimulus presentation; BS1: locomotion, n = 660 trials; BS2–BS5 stationary; BS2: >70% pupil size, n = 654; BS3: from 70% to 30%, n = 975; BS4: from 30% to 10%, n = 402; BS5: ≤10%, n = 237; 3 mice).

AAV, adeno-associated viral vector; CT, corticothalamic, dLGN, dorsal lateral geniculate nucleus; EEG, electroencephalogram; L6, layer 6; TC, thalamocortical; V1, primary visual cortex.

Please cite this article in press as: Augustinaite and Kuhn, Complementary Ca^{2+} Activity of Sensory Activated and Suppressed Layer 6 Corticothalamic Neurons Reflects Behavioral State, Current Biology (2020), https://doi.org/10.1016/j.cub.2020.07.069

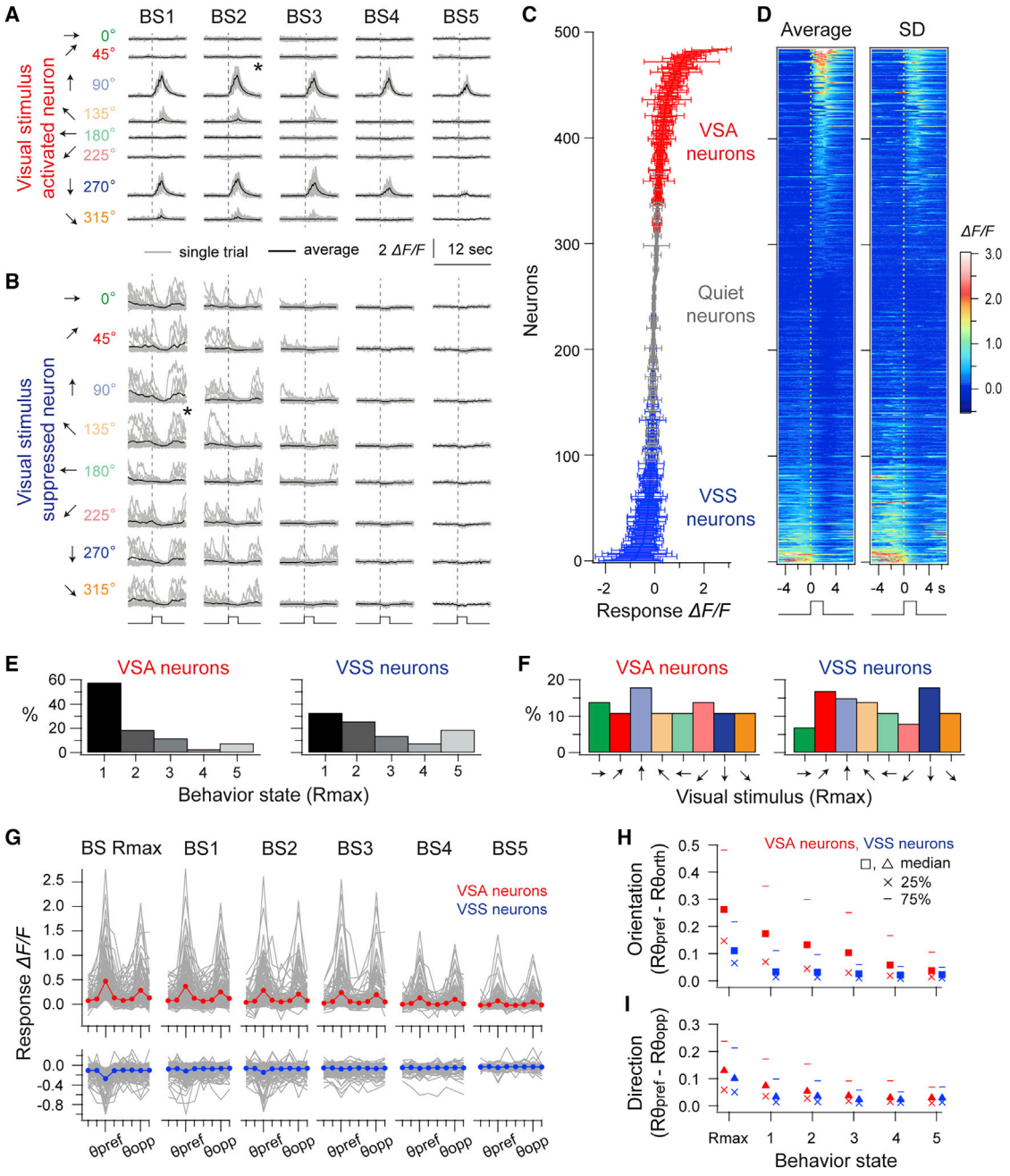

Figure 2. Visual Stimulus Activated (VSA), Visual Stimulus Suppressed (VSS), and Quiet L6 Corticothalamic Neurons

(A and B) Activity of (A) a VSA and (B) a VSS neuron in response to the 8 different visual stimuli directions during the 5 behavioral states (gray, single trial; black, average; n = 20 ± 13 trials per neuron). * indicates the strongest response elicited during the preferred condition, characterized by behavioral state and visual stimulus.

(C and D) Distribution (C) of the strongest responses elicited during the preferred condition of an individual neuron (average ± SD; n = 18 ± 14 trials per neuron; n = 485 neurons; 3 mice) and average (D) neuronal activity during the preferred condition (left) and corresponding SD (right); n the same as (C).

(E) Proportions of state preference among VSA and VSS neurons.

(F) Proportions of preferred directions among VSA and VSS neurons.

(G) Superimposed 360° tuning curves of a single VSA and VSS neuron (gray) and their average (red and blue) during a particular state. BS Rmax shows the tuning curves from the preferred behavioral state, when the maximum response (Rmax) is elicited. See also Figures S2 and S3.

(H and I) Orientation selectivity index (OSI) (H) and direction selectivity index (DSI) (I) of VSA (red) and VSS (blue) neurons; $R\theta_{pref}$, $R\theta_{orth}$, and $R\theta_{opp}$ are responses to the preferred, orthogonal, and opposite to the preferred stimulus directions, respectively; median, 25th and 75th percentiles. VSA n = 158, VSS n = 139.

Please cite this article in press as: Augustinaite and Kuhn, Complementary Ca^{2+} Activity of Sensory Activated and Suppressed Layer 6 Corticothalamic Neurons Reflects Behavioral State, Current Biology (2020), https://doi.org/10.1016/j.cub.2020.07.069

change with different state or stimulus (Figures 2A and 2B) but varied in a range, here described by the standard deviation (Figures 2C and 2D).

Surprisingly, Rmax behavioral state (BS Rmax) was different between different CTs (Figure 2E). More than half of VSAs responded most strongly during locomotion (BS1, 58%), and relatively few neurons were active during the least alertness states (BS4, 3% and BS5, 8%). In contrast, only 33% of VSSs were most strongly suppressed during locomotion, but larger fractions showed Rmax during drowsiness or sleep (BS4, 8% and BS5, 19%).

The direction angles of the Rmax eliciting gratings were approximately evenly distributed among CTs. About 13% of neurons within VSA or VSS group showed Rmax to one of the eight visual stimuli (Figure 2F).

Orientation Selectivity of L6CT Neurons

To characterize visual stimulus selectivity, tuning curves were calculated for individual CTs from average responses for 40 experimental conditions (8 stimuli × 5 states) and aligned at the preferred direction angle, eliciting the strongest response during the preferred state (BS Rmax preferred direction, θ_{pref}; Figures 2G and S2A). Orientation selectivity index (OSI) and direction selectivity index (DSI) were calculated for every state independently (Figures 2H and 2I). Based on the responses during the Rmax state, VSAs showed stronger selectivity to stimulus orientation than direction; meanwhile, inhibition of VSSs did not show a preference for orientation or direction (VSA BS Rmax OSI median: 0.26; DSI: 0.13, n = 158 pairs, $p < 0.001$; VSS BS Rmax OSI median: 0.11; DSI: 0.1, n = 139 pairs, $p = 0.464$; related-samples Wilcoxon signed rank test in both cases; Figures 2H and 2I). Orientation selectivity was significantly stronger for VSA than VSS neurons, but there was no difference between both groups for direction selectivity (BS Rmax OSI $p < 0.001$; BS Rmax DSI $p = 0.143$; n = 158 VSAs and 139 VSSs; independent-samples Mann-Whitney U test in both cases; Figures 2H and 2I).

The responses of CTs became weaker in less active behavioral states (Figures 2A, 2B, 2G, S2A, and S3). Due to this, OSI as well as DSI also decreased (VSA OSI and DSI, VSS OSI and DSI BS1–BS5, $p < 0.01$ in all cases; related-samples Friedman's two-way analysis of variance by ranks; in Figures 2H and 2I). However, despite weakening of selectivity, VSAs remained biased for a particular orientation, as indicated by their response peaks at θ_{pref} and θ_{opp} stimuli, corresponding to θ_{pref} and θ_{opp} of the preferred state, and a larger portion of neurons with these characteristic response peaks even during sleep (Figures 2G, S2, and S3A). In contrast, θ_{pref} of VSSs are close to random across states and did not match characteristics of the preferred state (Figures 2G, S2, and S3B), showing that suppression of these neurons is only weakly (if at all) tuned to a particular orientation or direction.

Diverse Activity Patterns of VSA and VSS Neurons

In addition to the behavior-state-related changes of the response amplitude (Figures 2A, 2G, S2A, and S3A), VSAs show a wide variety of visual-stimulus-driven activity in terms of selectivity, reliability, and response timing (e.g., selective and reliable On responses of N2 versus not selective responses with On and Off components of N1 or unreliable Off responses of N3 in Figures 3A and 3B). In contrast, VSSs exhibit not only amplitude (Figures 2B, 2G, S2A, and S3B) but also activity patterns linked to behavioral state (Figure 3C). For example, N1 is responsive when the mouse is active, i.e., running (BS1) or stationary (BS2), but quiet in less alert states, although N2 and N3 are only active when the mouse is alert but stationary (BS2) and N4 is mainly active during locomotion (BS1).

Interestingly, we find three different activity patterns within both VSA and VSS populations: neurons that are only active if the mouse sits still (lower rank neurons; Figures S4A and S4C), neurons which are active only during locomotion (lower rank neurons; Figures S4B and S4D), and neurons that do not discriminate between locomotion and stationary periods (high rank neurons; Figure S4).

Additionally, we calculated correlations (Spearman correlation coefficient; *rho* [ρ]) between the calcium signal $\Delta F/F$ and the two state-reflecting parameters: locomotion speed and pupil size (Figures 3E and 3F). To separate locomotion and state change effects, only episodes during which the mouse was stationary were used to estimate the neuronal activity correlation with pupil size.

The vast majority of VSA (91%) and VSS (83%) CTs increased their activity during more active behavior, indicated by larger pupil and/or higher running speed (groups 1–5; Figures 3E and 3F). However, although more than half of VSAs (60%) positively correlated with both pupil size and locomotion speed, this group was much smaller among VSSs (35%). The activity of some neurons positively correlated with only one parameter but showed no covariance with the other. For example, signals increased with larger pupil only (VSAs 25% and VSSs 33%), although for others, activity increased with faster locomotion only (VSAs 6% and VSSs 15%).

A larger group of VSSs (15%) than VSAs (7%) increased their activity with reduced alertness (groups 6–8; Figures 3E and 3F). The activity of 8% VSSs and 5% VSAs negatively correlated with both pupil size and locomotion speed. Also, 4% VSSs and 1% VSAs increased their activity with reduced pupil size but did not change with locomotion speed, although others became more active with slower locomotion but did not correlate with pupil size changes (VSAs 1% and VSSs 3%).

Neuronal activity of a small fraction of active CTs was not correlated (*rho* not significant; $p \geq 0.05$) with locomotion or pupil size (VSAs 1% and VSSs 2%; group 9; Figures 3E and 3F).

Complementary Activity of VSA and VSS Neurons Encodes Behavioral State

The population activity of both groups of CT neurons decreased with reduced alertness (Figures 1D, 2A, 2B, 2G, 4A, S2A, S3, and S4). Different direction gratings evoked very similar population responses within each state (Figure S5). Therefore, they were averaged and examined as pre- and post-stimulus onset activity (Figures 4B and S6). Consistent with positive correlations between neuronal activity and alertness (Figures 3E and 3F), the post-stimulus $\Delta F/F$ of VSAs was highest during locomotion and decreased for less active states, but the spontaneous pre-stimulus activity was low irrespectively of state (Figures 4A, 4B, and S6). Meanwhile pre-stimulus $\Delta F/F$ of VSSs was largest during high alertness and decreased toward less active states,

Please cite this article in press as: Augustinaite and Kuhn, Complementary Ca^{2+} Activity of Sensory Activated and Suppressed Layer 6 Corticothalamic Neurons Reflects Behavioral State, Current Biology (2020), https://doi.org/10.1016/j.cub.2020.07.069

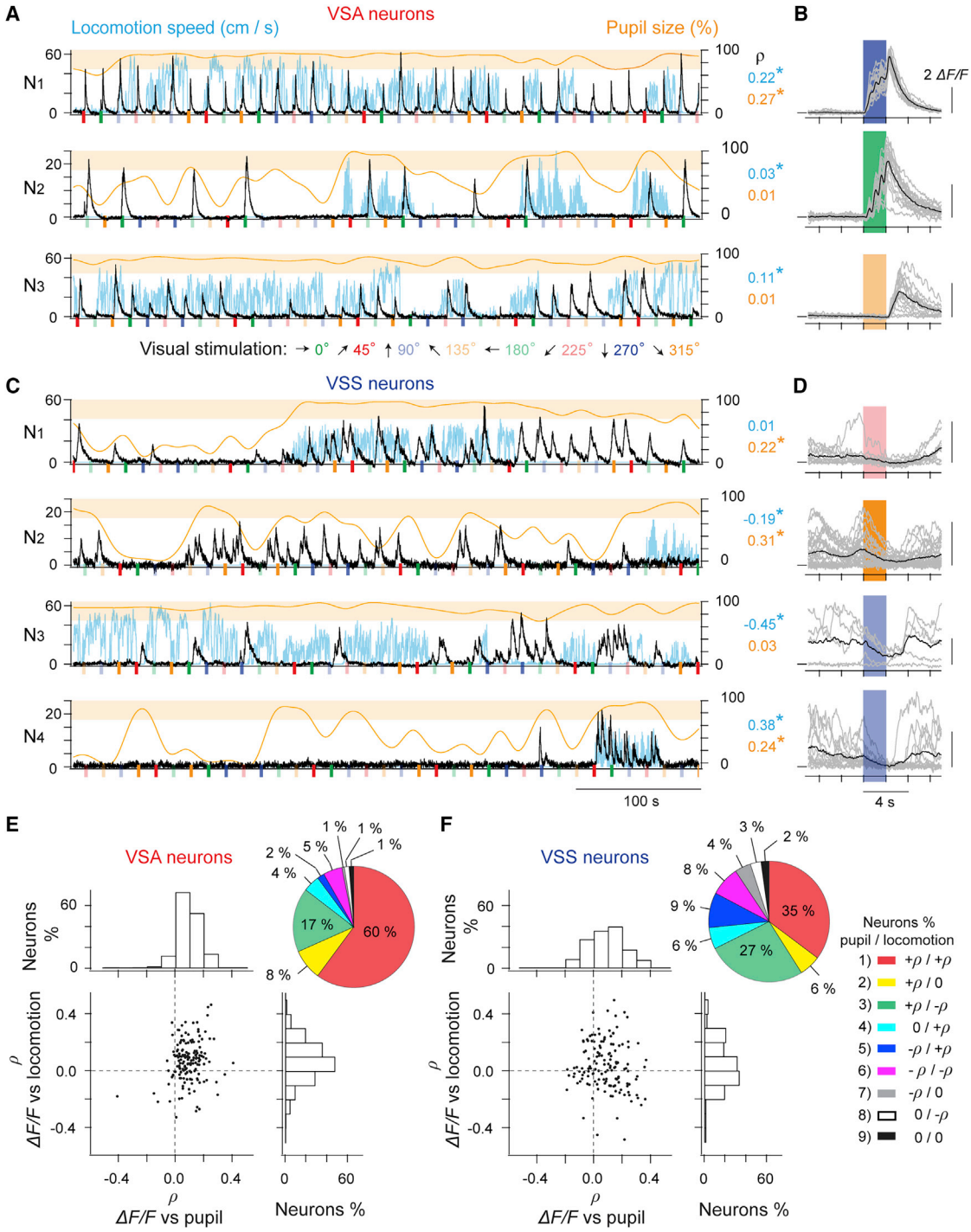

Figure 3. Diversity of Behavioral-State-Dependent Activity of L6 Corticothalamic Neurons

(A and C) Example calcium activity traces of individual neurons (black; 3 VSA neurons in A and 4 VSS neurons in C) superimposed with locomotion speed (blue) and normalized pre-stimulus pupil size (orange).

(B and D) Superimposed activity of (B) VSA and (D) VSS neurons (the same as in A and C) in response to the preferred visual stimulus during the preferred behavioral state (gray, single trial; black, average; B: N1: BS1, n = 19 trials; N2: BS1, n = 17; N3: BS1, n = 16; D: N1: BS1, n = 11; N2: BS2, n = 24; N3: BS2, n = 5 and N4: BS1, n = 13).

(E and F) Scatterplot of (E) VSA (n = 158) and (F) VSS (n = 139) neuronal activity versus locomotion speed and pupil size as well as projections showing both distributions. Pie charts: proportions of neurons based on their activity correlations with state parameters are shown.

Spearman correlation coefficient *rho* (ρ): positive (+), negative (−), or not significant (0; $p \geq 0.05$); * indicates significant correlation ($p < 0.05$) in (A) and (C). Light orange bar, pupil size >70% (BS2). See also Figure S4.

Please cite this article in press as: Augustinaite and Kuhn, Complementary Ca^{2+} Activity of Sensory Activated and Suppressed Layer 6 Corticothalamic Neurons Reflects Behavioral State, Current Biology (2020), https://doi.org/10.1016/j.cub.2020.07.069

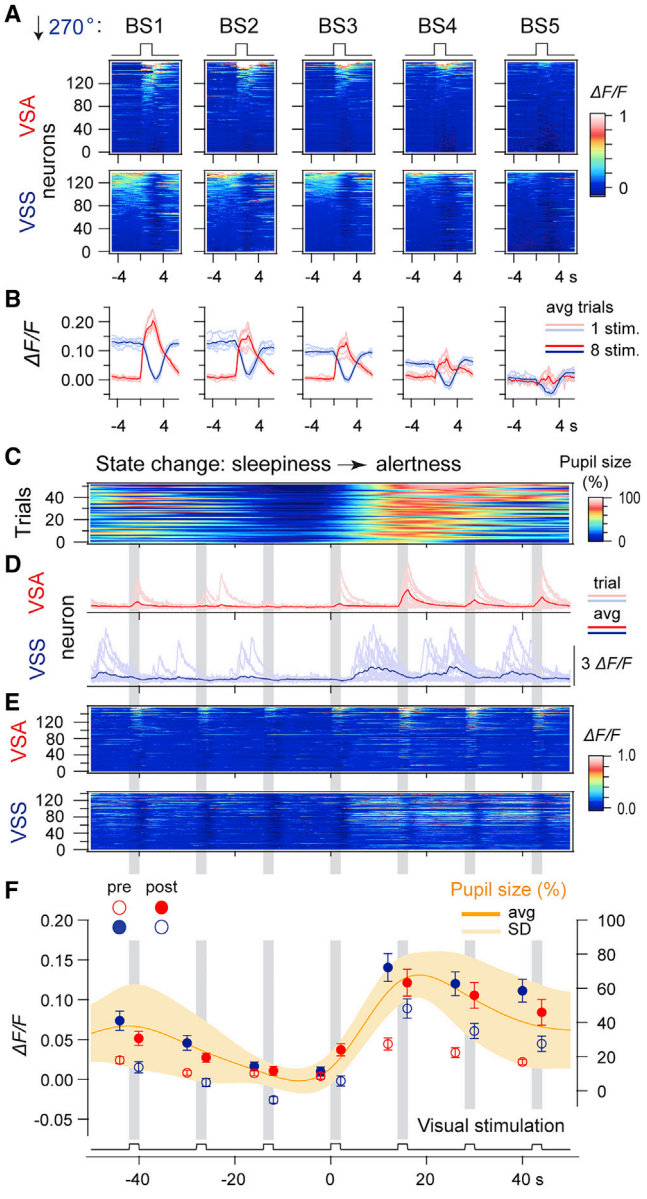

Figure 4. Behavioral-State-Dependent Changes of Complementary Calcium Activity of VSA and VSS Neurons

(A) Average neuronal activity with the presentation of one visual stimulus (270°) during different behavioral states; 158 VSA neurons; 139 VSS neurons; each panel was independently sorted; 23 ± 17 trials per neuron. See also Figure S5.

(B) Superimposed average activity of VSA (red) and VSS (blue) neurons in response to the presentation of 8 different directions (pale color traces) and their average. See also Figure S6.

(C) Temporally aligned segments of state change from sleep to wakefulness determined by change in pupil size.

(D) Examples of activity of a VSA (red) and a VSS (blue; n = 15 trials in both cases) neuron during the state change.

(E) Population activity of VSA and VSS neurons (n = 17 ± 8 trials per neuron).

(F) Superimposed time course of normalized pre-stimulus pupil size and average pre-stimulus and post-stimulus onset activity (4 s before and 4 s after; mean ± SEM) of VSA (red) and VSS (blue) neurons.

but post-stimulus activity was suppressed by the stimulus onset even during low-activity states (Figures 4A, 4B, and S6).

Although responses of VSAs were significantly stronger during BS1 than BS2, these two highest alertness states could not be separated in VSSs (VSA post-stimulus $p = 0.017$, $n = 158$; VSS pre-stimulus $p = 0.674$, post-stimulus onset $p = 0.093$, $n = 139$; related samples Wilcoxon signed rank test; Figure S6), probably reflecting larger groups of neurons active during either locomotion or stationary state (Figures 3C and S4).

We also collected time segments when the mouse remained stationary, but its behavioral state changed first to drowsiness or sleep and then to alertness (Figure 4C; see also STAR Methods). During the waking, on average, the pupil size increased from 8% ± 7% to 68% ± 13% ($n = 52$; Figures 4C and 4F).

The activity of both populations of CT neurons reflected the state change. Calcium activity was low during sleepiness and grew with increasing alertness (VSA Pearson $r = 0.7$ and VSS Pearson $r = 0.84$; in both cases, $n = 14$; $p < 0.001$; Figures 4D–4F). However, as during stimulus segments (Figures 4A and 4B), the activity of VSA and VSS neurons was alternating: VSSs dominated in the absence of a visual stimulus, although activity of VSAs dominated during visual stimulation (Figures 4D–4F). Due to such complementarity, the combined neuronal activity correlated even stronger with the alertness change (Pearson $r = 0.95$; $n = 14$; $p < 0.001$; VSS-pre and VSA-post; filled circles in Figure 4F) than the groups of VSAs and VSSs separately. In this way, L6 provides instantaneous state-related feedback to dLGN, mediated by two distinct but complementary populations of CT neurons.

The Relationship between Behavioral State, Pupil Size, and L6 Corticothalamic Activity

The pre-stimulus pupil size attenuates when behavior state changes from full alertness to sleep (Figures 1E and 1F), which leads to decrease of the retina illumination. It is not clear whether corticothalamic activity changes are reflecting changes in alertness, changes in pupil size, or both. To separate these two factors, we applied atropine on both eyes (~100 μL drop of 1% solution; 3 mice) after imaging under control condition for 1 h (Figure 5A). The experiment was resumed 30 min after the drug application, when the mouse recovered to normal behavior. The imaging sessions under atropine lasted for 1.5–2 h (Figure 5B).

The pupil size in both conditions was normalized to the maximal value during control, although EEG delta power was normalized to the absolute peak during the experiment (i.e., control or atropine). Even though the pupil dilation remained constant with atropine, the exposed pupil area decreased with reduced alertness due to closure of the eye lid (orange outline, Figure 5C). Two contrasting behavioral states were selected for the comparison: BS1 (locomotion) and BS4 (drowsiness). Atropine BS4 was defined for every mouse individually, using scaled (the range of min–max pupil values) control BS4 pupil size, because pupil size in both conditions showed similar relationship with EEG delta power (control 10%–30% corresponds to atropine 54%–70% range; Figure 5C). Neurons were divided into 3 groups, based on their response to 270° direction stimulus during control: positive (average response ≥ 0.1% $\Delta F/F$); weak

Please cite this article in press as: Augustinaite and Kuhn, Complementary Ca^{2+} Activity of Sensory Activated and Suppressed Layer 6 Corticothalamic Neurons Reflects Behavioral State, Current Biology (2020), https://doi.org/10.1016/j.cub.2020.07.069

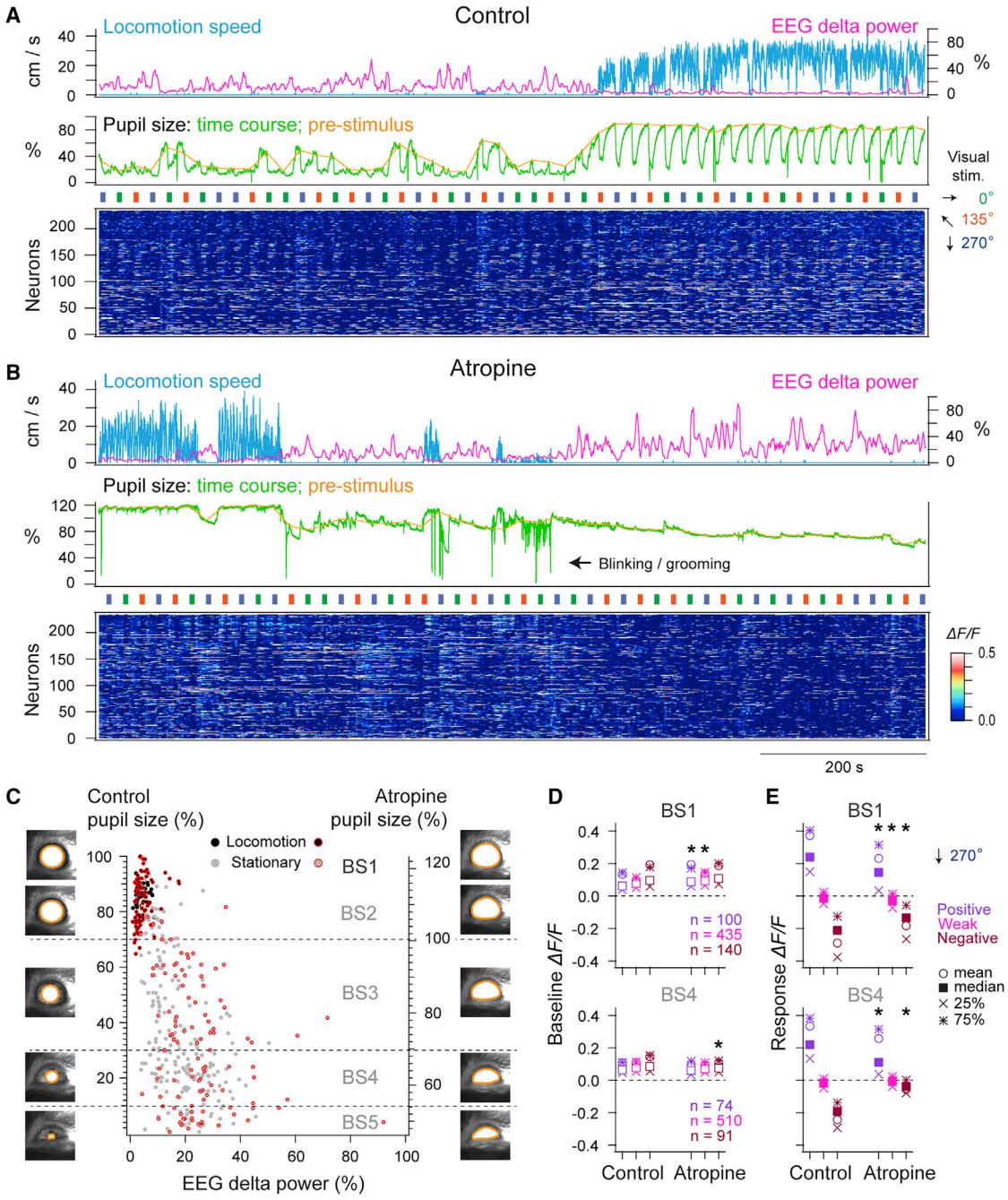

Figure 5. Relationship between Behavioral State, Pupil Size, and L6 Corticothalamic Activity

(A and B) Time course of behavioral state (top panel: locomotion speed [blue] and normalized EEG delta power [0.5–4 Hz, magenta]; middle panel: normalized exposed pupil size: time course [green] and extrapolated from pre-stimulus pupil size [orange]) with corresponding L6 corticothalamic activity (bottom panel: 235 neurons, 1 mouse) during (A) control (see also Videos S2 and S3) and (B) after atropine application. Visual stimuli (0°, 135°, and 270° full-screen drifting gratings and 2 Hz temporal and 0.08 cycles/deg spatial frequency) were presented in a random order for 5 s interleaved by 15-s dark screen intervals.

(C) Scatterplot of pre-stimulus exposed pupil size versus delta power used for the definition of the behavioral state (control: black/gray; atropine: black/gray with red outline; each dot indicates the behavioral state during a single visual stimulus presentation trial. BS1: locomotion, control n = 35 trials, atropine n = 84; BS2–BS5 stationary; BS2: control >70%, n = 29; atropine >100% pre-stimulus pupil size, n = 5; BS3: control from 70% to 30%, n = 71; atropine from 100% to 70%, n = 48; BS4: control from 30% to 10% pupil size, n = 74; atropine from 70% to 54%, n = 29; BS5: control pupil size ≤10%, n = 21; atropine ≤54%, n = 24, 1 mouse, the same as in A and B). The example images of the pupil (the exposed pupil area indicated with orange outline) during different states shown along the ordinates: left, during control; right, during atropine conditions.

(D and E) Baseline (D) and response (E) Δ*F*/*F* of positive (violet), weak (magenta), and negative (purple) neurons in control and atropine conditions during presentation of 270° direction full-screen drifting gratings; mean, median, 25th and 75th percentiles; top: behavioral state BS1; bottom: BS4. * indicates significantly different groups ($p < 0.05$; related samples Wilcoxon signed rank test) in (D) and (E).

Please cite this article in press as: Augustinaite and Kuhn, Complementary Ca^{2+} Activity of Sensory Activated and Suppressed Layer 6 Corticothalamic Neurons Reflects Behavioral State, Current Biology (2020), https://doi.org/10.1016/j.cub.2020.07.069

(<0.1% and >−0.1% Δ*F*/*F*); and negative (≤−0.1% Δ*F*/*F*). Sorting for BS1 and BS4 was done independently (Figure 5D).

On average, the pupil was about 29% (BS1) and 46% (BS4) larger with atropine (3 mice; BS1: control 85% ± 8% versus atropine 114% ± 7%, n = 79 and 180, respectively; BS4: control 21.3% ± 5% versus atropine 67% ± 11%, n = 179 and 93, respectively; $p < 0.001$, independent samples t test in both cases; Figure 5C). Additionally, the pupillary light response (calculated as difference between the pupil size before [average 1 s] and minimum size during the visual stimulus presentation [5 s]), strong during BS1 control, was reduced by 84%, and already weak during BS4 control—by 62% with atropine (3 mice; BS1: control 55% ± 10% versus atropine 9% ± 5%, n = 79 and 180, respectively, locomotion periods in Figures 5A and 5B; BS4: control 13% ± 5% [Figure 5A, left] versus atropine 5% ± 4% [Figure 5B, right], n = 179 and 93, respectively; $p < 0.001$; independent samples t test in both cases).

However, the larger exposed pupil area had no substantial effect on the baseline levels of activity nor lead to amplification of the responses to visual stimulation (Figures 5D and 5E). On the contrary, pupil dilation and pupillary light response removal resulted in overall reduction of the visually evoked activity. These results indicate that the corticothalamic population activity drop, observed during reduced alertness, did not reflect reduced pupil size and therefore lower illumination of the retina but was linked to the changes of the behavior state-related network activity.

L6 Corticothalamic Activity in the Absence of Visual Input

To assess what effect deprivation of visual stimuli has on the activity of L6CTs, we exposed mice (n = 2) to 3 different conditions: 1 h of visual stimulation as before (control), 30 min recording of spontaneous activity in total darkness (dark; mean luminance 0.00 cd m^{-2}), and 1 h of sensory stimulation as in control but with the retina inactivated by TTX (Figures 6A–6C). During the TTX experiment, the average pre- and post-stimulus *ΔF/F* was indistinguishable ($p = 0.911$; related-samples Wilcoxon signed rank test; n = 403), confirming that a visual stimulus had no effect on the activity of L6CTs under these conditions (Figure 6C). The behavioral state varied only between BS1 (locomotion) and BS2 (active stationary) during control and dark experiments. Only locomotion (artificially induced by treadmill rotation) or stationary were defined as states during the TTX experiment, because the mice had not recovered their normal behavior even 2 h after TTX injection. Neurons were categorized as VSA (34%, n = 136), quiet (43%, n = 174), or VSS (23%, n = 93; n = 2 mice) under control, as described earlier.

Although spontaneous activity of some neurons increased, the majority of VSAs became quiet after the visual stimulus elimination (dark: 85%; TTX: 64%; Figures 6A–6C, top). Most of quiet neurons also remained inactive in the absence of visual input (dark: 87%; TTX 66%; Figures 6A–6C, middle). The activity of VSS neurons was also substantially reduced (Figures 6A–6C, bottom). However, a larger group of active neurons within this population (dark: VSS 27% versus VSA 15%; TTX: VSS 61% versus VSA 36%) shows that VSSs were less affected by elimination of visual input and would contribute more to the L6CT feedback during these conditions than VSAs.

L6 Corticothalamic Activity Elicited by Different Visual Stimuli

Three different sets of visual stimuli were presented for 1 h each, to investigate the effect of different visual stimulus parameters (n = 2 mice): 8 directions full-screen drifting gratings as before (control; Figure 6D); 5 spatial frequencies full-screen drifting gratings (stimulation 2; Figure 6E); and full-field homogeneous illumination of 3 different light intensities (stimulation 3; Figure 6F).The behavioral state varied only between BS1 and BS3 during recording sessions. Neurons were categorized as VSA (44%, n = 167), quiet (25%, n = 95), or VSS (31%, n = 116) as described earlier, using responses elicited by control set of stimuli.

Even though a small group of active neurons "switched" their response type, that is, VSA became VSS (7% and 15%; Figures 6D–6F, top) or VSS became VSA (16% in both cases; Figures 6D–6F, bottom), the majority of the VSAs as well as VSSs showed either the same type of response or were not active when using other sets of stimuli (VSA 93% and 85%; VSS 84% in both cases; Figures 6D–6F, top and bottom). However, a relatively large fraction of quiet neurons became active in response to different grating frequencies or light intensities (as VSAs: 33% and 22% or VSSs: 9% and 13%; Figures 6D–6F, middle).

Morphology of VSA and VSS Neurons

To test for morphological differences between VSA and VSS neurons, we sparsely co-expressed tdTomato and GCaMP6f (n = 3 mice). Stacks were acquired with *in vivo* 2P microscopy, and thick dendrites were reconstructed. Consistent with previous studies [25, 26], we found neurons with a short apical dendrite and dendritic tuft in L4 and L3 and neurons with a long apical dendrite and tuft in L2 and L1 (Figure 7A).

Additionally, L6CTs were identified as VSA, quiet, or VSS by functional imaging (1 h per imaging plane) as in the core experiments described above. The behavioral state varied only between BS1 and BS3.

Short and long neuron types were found within each group of L6CTs (Figures 7B–7D). The dendritic length, approximated from the absolute height of the reconstruction, did not depend on the position within the layer (VSA somas at 640–730 μm cortical depth, Pearson r = 0.052, n = 12; quiet neurons: 640–730 μm, r = 0.055, n = 8; VSS: 650–740 μm, r = 0.016, n = 13; all r not significant [$p > 0.05$]; Figures 7B–7D).

However, on average, VSAs were taller than VSSs ($p = 0.001$; independent samples Mann-Whitney U test; Figure 7E). Also, reconstructions of apical dendrites of long VSAs often reached L1 and short VSAs could be traced up into L3 (neurons 1–8 and 11 and 12, respectively; Figure 7B). In contrast, only one long VSS neuron was approaching L1 and neurons with short apical dendrite could only be traced to about the middle of L4 (neurons 1 and 7–13, respectively; Figure 7D).

DISCUSSION

Three Populations of L6CT Neurons

Based on 2P calcium imaging experiments in V1 L6 in behaving head-fixed mice, we defined VSA and VSS neurons (VSA: 36.7% ± 6.4%, n = 462; VSS: 27.7% ± 4.2%, n = 348; n = 7 mice). About one-third of L6CTs (35.7% ± 9.5%, n = 457; n = 7

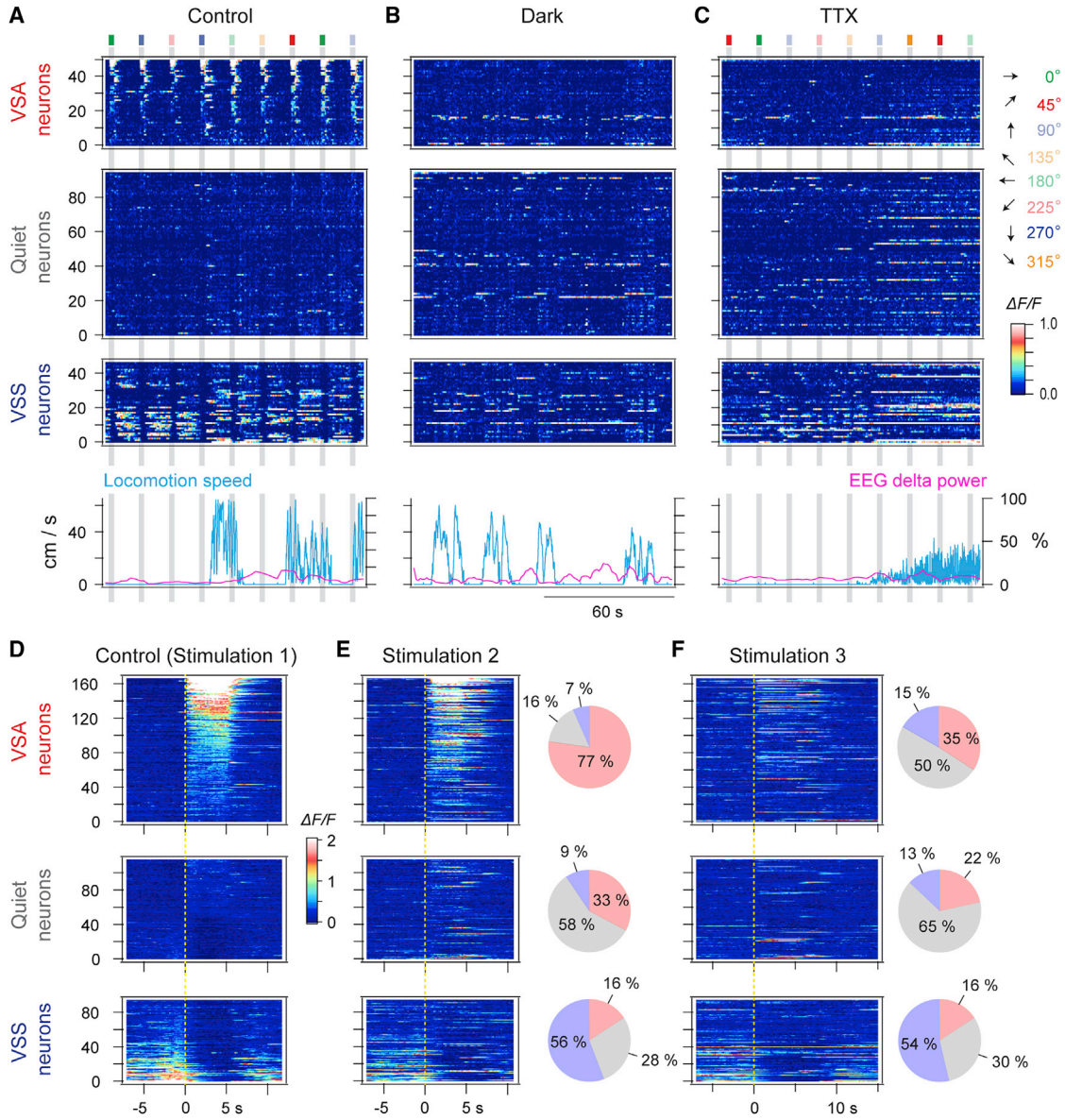

Figure 6. L6 Corticothalamic Activity during Different Stimulation Conditions

(A–C) Effect of sensory input elimination on population activity (192 neurons, 1 mouse) of VSA, quiet, and VSS neurons (A) control, i.e., standard visual stimulation experiment, (B) in total darkness (dark), and (C) under control condition of visual stimulation but 2 h after retinal inactivation by intraocular injection of TTX. Neurons are ranked according to their activity under control (A). Corresponding time course of behavioral state is shown (bottom panels): locomotion speed (blue) and normalized delta power (magenta). Note that locomotion was induced artificially in the TTX experiments.

(D–F) Effect of different visual stimuli (378 neurons, 2 mice): (D) control: full screen drifting gratings with 8 directions (step 45°; 0.08 cycles/deg spatial frequency) as in Figures 1, 2, 3, 4, and 5, except stimulus on was 5 s and stimulus off was 15 s; (E) stimulation 2: full-screen drifting gratings with 5 different spatial frequencies (0.01, 0.02, 0.04, 0.06, and 0.1 cycles/deg) and two different directions (0° and 270°) presented for 4 s with 14-s inter-trial intervals or for 6 s with 20 s inter-trials; (F) stimulation 3: full-screen homogeneous illumination with 3 different intensities (RGB blue: 100%, 50%, and 25%) presented for 5 s with 20-s inter-trial intervals or for 7.5 s with 30 s of inter-trials. For every neuron, the maximum response trials were selected and averaged (control: 2–14 [4 ± 2] trials per neuron; stimulation 2: 2–10 [3 ± 1] trials per neuron; stimulation 3: 2–27 [6 ± 6] trials per neuron). Neurons were sorted based on their response type (VSA, n = 167, top; quiet, n = 95, middle; and VSS, n = 116, bottom) and ranked according to their activity under control (D).

(E and F) Proportions of response types (pie chart: VSA, red; quiet, gray; VSS, blue) under respective stimulation compared to sorting under control (100%).

mice) remained quiet during control experiments. However, even these quiet neurons could show either VSA or VSS type of activity under different conditions (Figure 6) and thereby act as a pool for dynamic recruitment to one or another functional group. The idea that quiet neurons are just temporally non-responsive is also supported by the overlap of their distribution of dendritic length with the dendritic length distributions of both VSA and VSS neurons (Figure 7).

The VSAs showed orientation-tuned visual responses but otherwise very low spontaneous activity, as described before in

Please cite this article in press as: Augustinaite and Kuhn, Complementary Ca^{2+} Activity of Sensory Activated and Suppressed Layer 6 Corticothalamic Neurons Reflects Behavioral State, Current Biology (2020), https://doi.org/10.1016/j.cub.2020.07.069

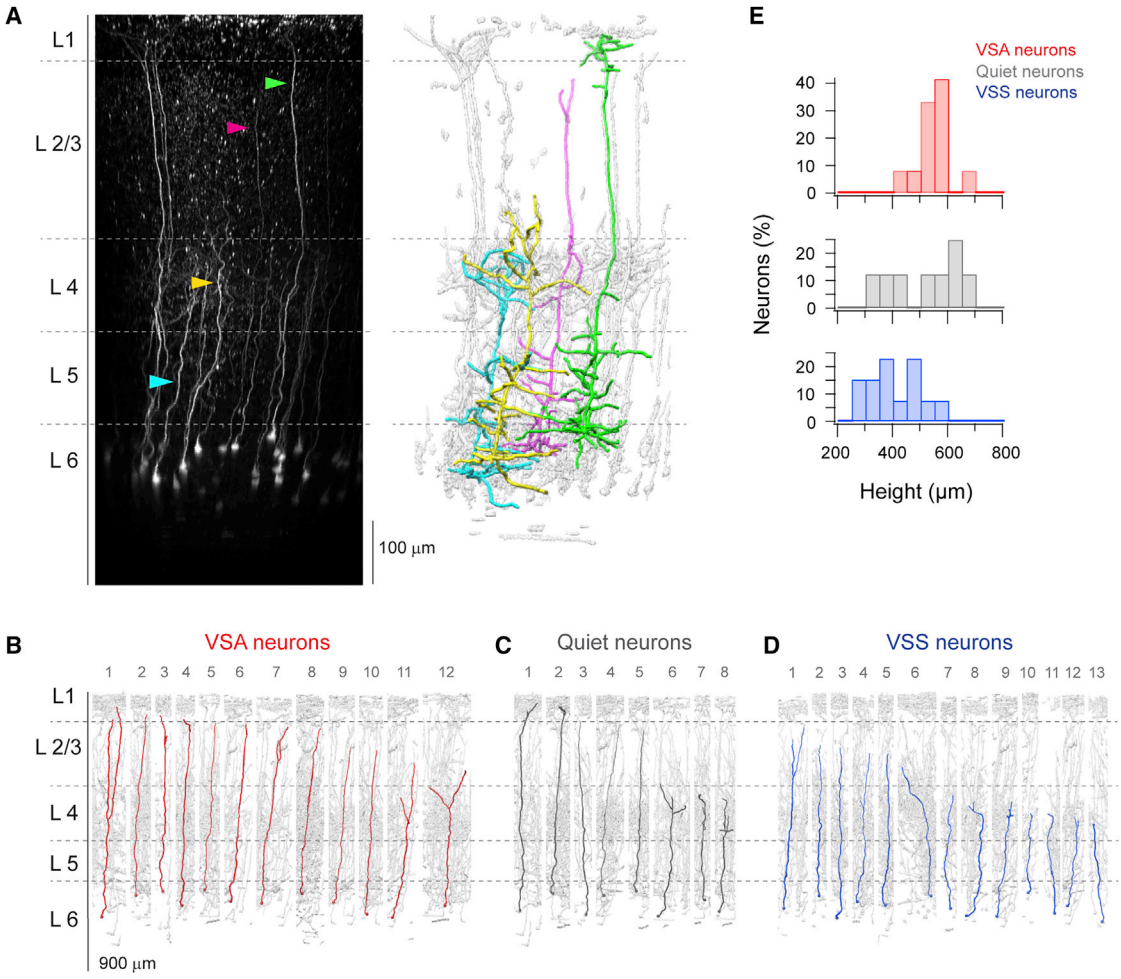

Figure 7. Morphology of VSA, Quiet, and VSS Corticothalamic Neurons

(A) *In vivo* 2P reconstruction of sparsely labeled CT neurons after injection of retrograde AAV.pCAG.Flex.tdTomato into dLGN (left) and 3D reconstruction of two short (yellow and cyan) and long (magenta and green) CT neurons.

(B–D) Basic reconstruction of (B) VSA, (C) Quiet, and (D) VSS neurons after identification by 2P calcium imaging.

(E) Distributions of reconstructed VSA (top; n = 12), Quiet (middle; n = 8), and VSS (bottom; n = 13) dendritic height. Gray background pattern (A–D) indicates the averaged labeling pattern of surrounding neurons to confirm the relative location of processes of reconstructed neurons.

V1 L6 of anesthetized mice [26, 41, 62, 63]. In contrast, the activity of VSSs was suppressed by visual stimulation. VSS neurons were spontaneously active in the absence of sensory input: in darkness as well as in TTX inactivated retina experiments. Therefore, it seems likely that VSSs activity is mainly driven by the cortico-cortical network, although intrinsic spontaneous firing or spontaneous thalamocortical activity [64] cannot be excluded.

The majority of corticothalamic neurons did not change their activity type during different conditions. The spontaneous activity levels, however, changed when passive viewing was replaced by visual deprivation (Figures 6A–6C). Activity of VSSs dropped, although VSA and quiet neurons became more active, presumably, as a consequence of the intra-cortical network activity change due to the absence of sensory input [65, 66]. Thus, the activity of L6CTs can be dynamically regulated by both cortical and sensory inputs.

Probably, VSSs were previously reported as suppressed-by-contrast neurons in retina and dLGN [67], visually non-responsive neurons in different layers of V1 [36, 62, 68–70], or as "silent-type" L6CTs that were suppressed during tone presentation in primary auditory cortex (A1) [71]. This indicates that sensory-activated and suppressed neurons, most likely, are not a special feature of V1 L6 but might also be present in the sensory periphery, thalamus, and other layers of primary or even higher order cortices.

We found short and tall morphology types [25, 26] among functionally identified VSA and VSS CTs. However, in our reconstructions, VSAs were on average taller than VSSs. Many VSAs had their apical tuft in L1, although most VSSs did not, and their processes remained within L4. Such anatomical differences suggest functionally different bottom-up as well as top-down signal integration circuits.

VSAs, like other sensory pyramidal neurons, receive monosynaptic thalamic excitation in L6 and L4 [27, 71, 72]. VSSs also receive excitatory thalamic input, but it is relatively weak and polysynaptically relayed from other cortical neurons [71].

Please cite this article in press as: Augustinaite and Kuhn, Complementary Ca^{2+} Activity of Sensory Activated and Suppressed Layer 6 Corticothalamic Neurons Reflects Behavioral State, Current Biology (2020), https://doi.org/10.1016/j.cub.2020.07.069

Moreover, thalamic input causes strong feedforward inhibition in L6 and L4 [17, 73, 74], which can explain the powerful silencing of VSSs during sensory processing. L6CTs also receive dense local and long-range cortical inputs within L6 [1, 2, 39–41], which might be the main state-related excitatory drive for short VSSs and VSAs. Tall VSAs, additionally, can integrate primary and higher order thalamic input [28–30] as well as top-down feedback from higher cortical areas in L1 [39, 40]. Together with cortical inputs within L6, these projections could tune tall VSAs for optimal behavior state and perceptual context-dependent processing of sensory signals [30, 31, 33, 43, 45, 47].

We classified L6CTs into 3 groups: VSA; VSS; and quiet neurons. However, the distribution of responses is a continuum (Figures 2C and 2D), and therefore, any classification is, to some extent, artificial. The neurons could be further grouped according to their specific activity patterns, for example, visual On versus Off responses or preference of locomotion versus stationary periods (Figures 3 and S4). Also, the receptive field structure, not studied here, could provide additional information important for classification.

L6 Corticothalamic Activity during Different Behavioral States

Multiple brain areas, including brainstem, basal forebrain, and hypothalamus, using various neurotransmitters, through local and long-range circuits to cortex and subcortical areas, are controlling the ongoing changes of the brain state, reflected in continuously adapting animal behavior [23, 24, 61, 75, 76]. In contrast to other cortical layers, L6 appears to be especially susceptible to acetylcholine (ACh) and orexin/hypocretin [77], neurotransmitters that play pivotal roles during sleep-wake transitions and wakefulness. The importance of ACh was suggested by dense basal forebrain projections in L6 [78], by high expression levels of muscarinic and nicotinic ACh receptors in L6CTs, and by their excitation via these receptors [79]. Interestingly, orexin-/hypocretin-induced responses were observed exclusively in L6B [80]. How these neurons affect L6A is unknown. However, it was suggested that orexin-sensitive L6B neurons can regulate activity of L6A in relation to wakefulness as they predominantly innervate neurons in L5 and L6 [80].

We found that the activity of V1 L6CTs correlates with behavioral state: the average population activity is higher during vigilance and locomotion and decreases with drowsiness and sleep, like activity of neurons in the upper layers of V1 [34–38, 70]. As had been shown earlier [70], arousal facilitated visual responses of L6CTs as well as center-surround suppression, that is, the activity of interneurons [81]. Thus, behavior-state- and visual-stimulation-induced activity of interneurons [70, 82] could explain state-related suppression of VSSs and, possibly, the negative calcium transients of VSSs during inactive periods (Figures 2B, 4A, and 4B). Such signals were reported before [83], representing subthreshold membrane potential fluctuations in dendrites and soma.

The cellular resolution revealed state-related heterogeneity among VSAs and especially among VSSs (neurons active during sleep [38] or neurons active only during stationary periods). Further investigations are necessary to define exact circuitries underlying such diversity of activity patterns.

Most importantly, the activity of VSA and VSS populations is complementary: if VSAs are activated during vision, VSSs are suppressed. And opposite, VSAs are quiet in the absence of a visual stimulus and VSSs show an average activity level similar to that of active VSAs. Thereby, the average output to thalamus (detected by calcium imaging) is kept relatively constant during a particular behavioral state.

Our findings are consistent with the notion that it is not the average activity of all the individual cells but distinct sub-populations or ensembles of neurons that form emerging functional units [84]. Such functional subnetworks, emerging during spontaneous as well as sensory- or task-driven behavior, have been observed in subcortical and different cortical areas [48–50, 85]. We show that, even when the average population activity is low and the activity of individual neurons is sparse, there is always a dedicated sub-population of neurons adequately responding to sensory inputs and/or internal network states.

Pupil size is widely used as indicator of the brain state because it reflects the dynamics of cortical networks [59] as well as activity changes in adrenergic and cholinergic neuromodulatory systems [86]. Even with atropine, when the pupil was maximally dilated, the effective pupil size still dropped proportionally with reduced alertness, due the closure of the eye lid, resulting in a pupil size / EEG relationship comparable to control (Figure 5C) or the one reported, for example, in A1 [59]. However, pupil size variations are directly driven by environmental light intensity, leading to changes in retinal illumination and, accordingly, changes in responsiveness along the visual pathway [87]. We found that the activity of L6CTs did not increase with larger pupil size, indicating that these neurons are insensitive to the absolute pupil size and retinal illumination but reflect the behavior state. This finding might be relevant to neurons of all cortical layers of V1, because correlation between pupil size and activity changes persisted in V1 L2/3 of FVB mice in which retinal ganglion cells degenerate in adulthood [35].

Proposed Effect of L6 Corticothalamic Activity on Thalamus

Importantly, the corticothalamic projections from L6 are not the only pathway of state-dependent regulation of thalamic activity. In addition to cortical feedback, intrinsic properties of TCs (T-type Ca^{2+} channels), feedforward, and feedback inhibition as well as direct cholinergic and adrenergic regulation from brainstem and other neuromodulatory systems [4, 7, 21–23] shape thalamocortical activity in a behavior-dependent manner [8, 88]. During vision, feedback carried by VSAs will provide sensory and state information, relevant to ongoing demands of visual perception. At other times, the information about the current behavioral state will be mediated by VSSs and, in particular conditions, e.g., longer absence of sensory input, by spontaneously active VSA neurons.

Primary sensory cortex L6CTs dynamically regulate activity of both primary and higher order thalamic nuclei [19] (dLGN and lateral posterior nucleus [LP] in the visual system). However, these two projections have different sublaminar sources: CTs from the upper sublayer send axons only to dLGN, although those from the lower project to dLGN and LP [89, 90]. In addition to thalamic targets, these sublayers have a distinct synaptic organization [91] that can differentially influence the output of

Please cite this article in press as: Augustinaite and Kuhn, Complementary Ca^{2+} Activity of Sensory Activated and Suppressed Layer 6 Corticothalamic Neurons Reflects Behavioral State, Current Biology (2020), https://doi.org/10.1016/j.cub.2020.07.069

L6CTs. We found VSA and VSS neurons throughout L6 (Figure 7). However, additional experiments are necessary to determine whether and how L6 feedback to primary thalamus is different from feedback to higher order thalamus.

In theory, the effect of corticothalamic input on TCs can vary from excitation to inhibition: excitatory projections synapse not only on TC neurons but also on GABA-ergic neurons of thalamic reticular nucleus and, in case of dLGN, intrinsic interneurons. The strength of net excitation versus inhibition depends on a dynamic and frequency-dependent interplay of changes in synaptic properties in the circuitry [16, 18]. A recent study showed that sustained photostimulation of L6CTs suppresses; however, moderate frequency (10 Hz) powerfully facilitates thalamic activity in awake animals [19]. We find strongest activity during highest alertness states. However, even then, the activity is relatively sparse and is mediated by only a fraction of CTs (Figures 1D, 3, and 4). Thus, it is unlikely that CT feedback could trigger strong sustained inhibition onto TC neurons. Unfortunately, calcium signals cannot be simply converted to the action potentials. Most likely, sparse trains or bursts of action potentials underly the positive calcium transients of VSAs and VSSs, as shown in other cortical pyramidal neurons [83, 92]. However, further experiments, for example with voltage imaging, are necessary to answer long-standing questions about firing frequencies of L6CTs during behavior.

Possibly, VSAs provide retinotopic projections to thalamus, as is necessary for receptive field organization and optimal processing of sensory signal [5, 93], although projections of VSSs are not specific because these neurons do not code any parameter of the sensory signal. Different axonal conduction velocities (lower for visually non-responsive CTs) [70, 94] could be another indicator of functionally different corticothalamic channels [5]. However, so far, there is no evidence pointing toward dichotomy in the projection patterns or the synaptic properties of corticothalamic synapses. Corticothalamic projections show a high degree of convergence on distal dendrites of TC neurons in dLGN [3, 4]. Here, presynaptic activity of CTs can trigger dendritic NMDA plateau potentials [14] and thereby, through sustained depolarization, switch TC neurons from bursting to regular firing and can amplify retinogeniculate transfer when in a regular firing mode. We speculate that, with this mechanism, L6CTs can continuously control the membrane depolarization level of TC neurons, depending on behavioral state, and thereby regulate information flow from retina to cortex.

STAR★METHODS

Detailed methods are provided in the online version of this paper and include the following:

- KEY RESOURCES TABLE
- RESOURCE AVAILABILITY
  - Lead Contact
  - Materials Availability
  - Data and Code Availability
- EXPERIMENTAL MODEL AND SUBJECT DETAILS
  - Animals
- METHOD DETAILS
  - Chronic cranial window surgery
  - AAV injection to label dLGN axonal projections
  - Retrograde tracer injection
  - Retrograde AAV injection to sparsely label dLGN-projecting L6CT neurons
  - Viral injection through the port of the cranial window
  - Intravitreal TTX injection
  - Ophthalmic application of Atropine
  - Visual stimulation
  - Intrinsic signal imaging
  - Two photon calcium imaging and behavioral state recording
- QUANTIFICATION AND STATISTICAL ANALYSIS
  - Ca^{2+} imaging analysis
  - Behavioral state characterization and data sorting

SUPPLEMENTAL INFORMATION

Supplemental Information can be found online at https://doi.org/10.1016/j.cub.2020.07.069.

ACKNOWLEDGMENTS

The authors thank Kazuo Mori (OIST) and Ray Lee (OIST) for technical support. This work was supported by JSPS KAKENHI Grant Number 17K14941 to S.A. and the OIST Graduate University.

AUTHOR CONTRIBUTIONS

S.A. and B.K. designed the research, S.A. conducted the experiments and analyzed the data, and S.A. and B.K. wrote the manuscript.

DECLARATION OF INTERESTS

The authors declare no competing interests.

Received: February 12, 2020
Revised: June 12, 2020
Accepted: July 22, 2020
Published: August 20, 2020

REFERENCES

1. Briggs, F. (2010). Organizing principles of cortical layer 6. Front. Neural Circuits *4*, 3.
2. Thomson, A.M. (2010). Neocortical layer 6, a review. Front. Neuroanat. *4*, 13.
3. Jones, E.G. (2007). The Thalamus*Volume 1*, Second Edition (Cambridge University).
4. Sherman, S.M., and Guillery, R.W. (2006). Exploring the Thalamus and Its Role in Cortical Function, Second Edition (The MIT Press).
5. Briggs, F., and Usrey, W.M. (2008). Emerging views of corticothalamic function. Curr. Opin. Neurobiol. *18*, 403–407.
6. Sillito, A.M., and Jones, H.E. (2002). Corticothalamic interactions in the transfer of visual information. Philos. Trans. R. Soc. Lond. B Biol. Sci. *357*, 1739–1752.
7. Castro-Alamancos, M.A. (2004). Dynamics of sensory thalamocortical synaptic networks during information processing states. Prog. Neurobiol. *74*, 213–247.
8. Usrey, W.M., and Alitto, H.J. (2015). Visual functions of the thalamus. Annu. Rev. Vis. Sci. *1*, 351–371.
9. Hasse, J.M., and Briggs, F. (2017). Corticogeniculate feedback sharpens the temporal precision and spatial resolution of visual signals in the ferret. Proc. Natl. Acad. Sci. USA *114*, E6222–E6230.

Please cite this article in press as: Augustinaite and Kuhn, Complementary Ca^{2+} Activity of Sensory Activated and Suppressed Layer 6 Corticothalamic Neurons Reflects Behavioral State, Current Biology (2020), https://doi.org/10.1016/j.cub.2020.07.069

10. Eyding, D., Macklis, J.D., Neubacher, U., Funke, K., and Wörgötter, F. (2003). Selective elimination of corticogeniculate feedback abolishes the electroencephalogram dependence of primary visual cortical receptive fields and reduces their spatial specificity. J. Neurosci. *23*, 7021–7033.

11. Wang, W., Andolina, I.M., Lu, Y., Jones, H.E., and Sillito, A.M. (2018). Focal gain control of thalamic visual receptive fields by layer 6 corticothalamic feedback. Cereb. Cortex *28*, 267–280.

12. Guo, W., Clause, A.R., Barth-Maron, A., and Polley, D.B. (2017). A corticothalamic circuit for dynamic switching between feature detection and discrimination. Neuron *95*, 180–194.e5.

13. Pauzin, F.P., and Krieger, P. (2018). A corticothalamic circuit for refining tactile encoding. Cell Rep. *23*, 1314–1325.

14. Augustinaite, S., Kuhn, B., Helm, P.J., and Heggelund, P. (2014). NMDA spike/plateau potentials in dendrites of thalamocortical neurons. J. Neurosci. *34*, 10892–10905.

15. Mease, R.A., Krieger, P., and Groh, A. (2014). Cortical control of adaptation and sensory relay mode in the thalamus. Proc. Natl. Acad. Sci. USA *111*, 6798–6803.

16. Crandall, S.R., Cruikshank, S.J., and Connors, B.W. (2015). A corticothalamic switch: controlling the thalamus with dynamic synapses. Neuron *86*, 768–782.

17. Cruikshank, S.J., Urabe, H., Nurmikko, A.V., and Connors, B.W. (2010). Pathway-specific feedforward circuits between thalamus and neocortex revealed by selective optical stimulation of axons. Neuron *65*, 230–245.

18. Augustinaite, S., Yanagawa, Y., and Heggelund, P. (2011). Cortical feedback regulation of input to visual cortex: role of intrageniculate interneurons. J. Physiol. *589*, 2963–2977.

19. Kirchgessner, M.A., Franklin, A.D., and Callaway, E.M. (2020). Context-dependent and dynamic functional influence of corticothalamic pathways to first- and higher-order visual thalamus. Proc. Natl. Acad. Sci. USA *117*, 13066–13077.

20. Harris, K.D., and Shepherd, G.M. (2015). The neocortical circuit: themes and variations. Nat. Neurosci. *18*, 170–181.

21. McCormick, D.A., McGinley, M.J., and Salkoff, D.B. (2015). Brain state dependent activity in the cortex and thalamus. Curr. Opin. Neurobiol. *31*, 133–140.

22. Steriade, M. (2000). Corticothalamic resonance, states of vigilance and mentation. Neuroscience *101*, 243–276.

23. McCormick, D.A., and Bal, T. (1997). Sleep and arousal: thalamocortical mechanisms. Annu. Rev. Neurosci. *20*, 185–215.

24. Lee, S.H., and Dan, Y. (2012). Neuromodulation of brain states. Neuron *76*, 209–222.

25. Gouwens, N.W., Sorensen, S.A., Berg, J., Lee, C., Jarsky, T., Ting, J., Sunkin, S.M., Feng, D., Anastassiou, C.A., Barkan, E., et al. (2019). Classification of electrophysiological and morphological neuron types in the mouse visual cortex. Nat. Neurosci. *22*, 1182–1195.

26. Olsen, S.R., Bortone, D.S., Adesnik, H., and Scanziani, M. (2012). Gain control by layer six in cortical circuits of vision. Nature *483*, 47–52.

27. Constantinople, C.M., and Bruno, R.M. (2013). Deep cortical layers are activated directly by thalamus. Science *340*, 1591–1594.

28. Rubio-Garrido, P., Pérez-de-Manzo, F., Porrero, C., Galazo, M.J., and Clascá, F. (2009). Thalamic input to distal apical dendrites in neocortical layer 1 is massive and highly convergent. Cereb. Cortex *19*, 2380–2395.

29. Cruz-Martín, A., El-Danaf, R.N., Osakada, F., Sriram, B., Dhande, O.S., Nguyen, P.L., Callaway, E.M., Ghosh, A., and Huberman, A.D. (2014). A dedicated circuit links direction-selective retinal ganglion cells to the primary visual cortex. Nature *507*, 358–361.

30. Roth, M.M., Dahmen, J.C., Muir, D.R., Imhof, F., Martini, F.J., and Hofer, S.B. (2016). Thalamic nuclei convey diverse contextual information to layer 1 of visual cortex. Nat. Neurosci. *19*, 299–307.

31. Erisken, S., Vaiceliunaite, A., Jurjut, O., Fiorini, M., Katzner, S., and Busse, L. (2014). Effects of locomotion extend throughout the mouse early visual system. Curr. Biol. *24*, 2899–2907.

32. Saalmann, Y.B., Pinsk, M.A., Wang, L., Li, X., and Kastner, S. (2012). The pulvinar regulates information transmission between cortical areas based on attention demands. Science *337*, 753–756.

33. Halassa, M.M., and Kastner, S. (2017). Thalamic functions in distributed cognitive control. Nat. Neurosci. *20*, 1669–1679.

34. Vinck, M., Batista-Brito, R., Knoblich, U., and Cardin, J.A. (2015). Arousal and locomotion make distinct contributions to cortical activity patterns and visual encoding. Neuron *86*, 740–754.

35. Reimer, J., Froudarakis, E., Cadwell, C.R., Yatsenko, D., Denfield, G.H., and Tolias, A.S. (2014). Pupil fluctuations track fast switching of cortical states during quiet wakefulness. Neuron *84*, 355–362.

36. Niell, C.M., and Stryker, M.P. (2010). Modulation of visual responses by behavioral state in mouse visual cortex. Neuron *65*, 472–479.

37. Bennett, C., Arroyo, S., and Hestrin, S. (2013). Subthreshold mechanisms underlying state-dependent modulation of visual responses. Neuron *80*, 350–357.

38. Senzai, Y., Fernandez-Ruiz, A., and Buzsáki, G. (2019). Layer-specific physiological features and interlaminar interactions in the primary visual cortex of the mouse. Neuron *101*, 500–513.e5.

39. Felleman, D.J., and Van Essen, D.C. (1991). Distributed hierarchical processing in the primate cerebral cortex. Cereb. Cortex *1*, 1–47.

40. Callaway, E.M. (2004). Feedforward, feedback and inhibitory connections in primate visual cortex. Neural Netw. *17*, 625–632.

41. Vélez-Fort, M., Rousseau, C.V., Niedworok, C.J., Wickersham, I.R., Rancz, E.A., Brown, A.P.Y., Strom, M., and Margrie, T.W. (2014). The stimulus selectivity and connectivity of layer six principal cells reveals cortical microcircuits underlying visual processing. Neuron *84*, 238.

42. Vélez-Fort, M., Bracey, E.F., Keshavarzi, S., Rousseau, C.V., Cossell, L., Lenzi, S.C., Strom, M., and Margrie, T.W. (2018). A circuit for integration of head- and visual-motion signals in layer 6 of mouse primary visual cortex. Neuron *98*, 179–191.e6.

43. Gilbert, C.D., and Li, W. (2013). Top-down influences on visual processing. Nat. Rev. Neurosci. *14*, 350–363.

44. Larkum, M. (2013). A cellular mechanism for cortical associations: an organizing principle for the cerebral cortex. Trends Neurosci. *36*, 141–151.

45. Zhang, S., Xu, M., Kamigaki, T., Hoang Do, J.P., Chang, W.C., Jenvay, S., Miyamichi, K., Luo, L., and Dan, Y. (2014). Selective attention. Long-range and local circuits for top-down modulation of visual cortex processing. Science *345*, 660–665.

46. Kuhn, B., Denk, W., and Bruno, R.M. (2008). In vivo two-photon voltage-sensitive dye imaging reveals top-down control of cortical layers 1 and 2 during wakefulness. Proc. Natl. Acad. Sci. USA *105*, 7588–7593.

47. Nurminen, L., Merlin, S., Bijanzadeh, M., Federer, F., and Angelucci, A. (2018). Top-down feedback controls spatial summation and response amplitude in primate visual cortex. Nat. Commun. *9*, 2281.

48. Funamizu, A., Kuhn, B., and Doya, K. (2016). Neural substrate of dynamic Bayesian inference in the cerebral cortex. Nat. Neurosci. *19*, 1682–1689.

49. Stringer, C., Pachitariu, M., Steinmetz, N., Reddy, C.B., Carandini, M., and Harris, K.D. (2019). Spontaneous behaviors drive multidimensional, brainwide activity. Science *364*, 255.

50. Miller, J.E., Ayzenshtat, I., Carrillo-Reid, L., and Yuste, R. (2014). Visual stimuli recruit intrinsically generated cortical ensembles. Proc. Natl. Acad. Sci. USA *111*, E4053–E4061.

51. Gong, S., Doughty, M., Harbaugh, C.R., Cummins, A., Hatten, M.E., Heintz, N., and Gerfen, C.R. (2007). Targeting Cre recombinase to specific neuron populations with bacterial artificial chromosome constructs. J. Neurosci. *27*, 9817–9823.

52. Roome, C.J., and Kuhn, B. (2014). Chronic cranial window with access port for repeated cellular manipulations, drug application, and electrophysiology. Front. Cell. Neurosci. *8*, 379.

53. Schuett, S., Bonhoeffer, T., and Hübener, M. (2002). Mapping retinotopic structure in mouse visual cortex with optical imaging. J. Neurosci. *22*, 6549–6559.

54. Theer, P., and Denk, W. (2006). On the fundamental imaging-depth limit in two-photon microscopy. J. Opt. Soc. Am. A Opt. Image Sci. Vis. *23*, 3139–3149.

55. Helmchen, F., and Denk, W. (2005). Deep tissue two-photon microscopy. Nat. Methods *2*, 932–940.

56. Roome, C.J., and Kuhn, B. (2018). Simultaneous dendritic voltage and calcium imaging and somatic recording from Purkinje neurons in awake mice. Nat. Commun. *9*, 3388.

57. Polack, P.O., Friedman, J., and Golshani, P. (2013). Cellular mechanisms of brain state-dependent gain modulation in visual cortex. Nat. Neurosci. *16*, 1331–1339.

58. Lee, A.M., Hoy, J.L., Bonci, A., Wilbrecht, L., Stryker, M.P., and Niell, C.M. (2014). Identification of a brainstem circuit regulating visual cortical state in parallel with locomotion. Neuron *83*, 455–466.

59. McGinley, M.J., David, S.V., and McCormick, D.A. (2015). Cortical membrane potential signature of optimal states for sensory signal detection. Neuron *87*, 179–192.

60. Yüzgeç, O., Prsa, M., Zimmermann, R., and Huber, D. (2018). Pupil size coupling to cortical states protects the stability of deep sleep via parasympathetic modulation. Curr. Biol. *28*, 392–400.e3.

61. McGinley, M.J., Vinck, M., Reimer, J., Batista-Brito, R., Zagha, E., Cadwell, C.R., Tolias, A.S., Cardin, J.A., and McCormick, D.A. (2015). Waking state: rapid variations modulate neural and behavioral responses. Neuron *87*, 1143–1161.

62. Niell, C.M., and Stryker, M.P. (2008). Highly selective receptive fields in mouse visual cortex. J. Neurosci. *28*, 7520–7536.

63. Denman, D.J., and Contreras, D. (2015). Complex effects on in vivo visual responses by specific projections from mouse cortical layer 6 to dorsal lateral geniculate nucleus. J. Neurosci. *35*, 9265–9280.

64. Linden, M.L., Heynen, A.J., Haslinger, R.H., and Bear, M.F. (2009). Thalamic activity that drives visual cortical plasticity. Nat. Neurosci. *12*, 390–392.

65. Poulet, J.F., Fernandez, L.M., Crochet, S., and Petersen, C.C. (2012). Thalamic control of cortical states. Nat. Neurosci. *15*, 370–372.

66. Hirata, A., and Castro-Alamancos, M.A. (2010). Neocortex network activation and deactivation states controlled by the thalamus. J. Neurophysiol. *103*, 1147–1157.

67. Jacoby, J., and Schwartz, G.W. (2018). Typology and circuitry of suppressed-by-contrast retinal ganglion cells. Front. Cell. Neurosci. *12*, 269.

68. Hirsch, J.A., Gallagher, C.A., Alonso, J.M., and Martinez, L.M. (1998). Ascending projections of simple and complex cells in layer 6 of the cat striate cortex. J. Neurosci. *18*, 8086–8094.

69. Stoelzel, C.R., Bereshpolova, Y., Alonso, J.M., and Swadlow, H.A. (2017). Axonal conduction delays, brain state, and corticogeniculate communication. J. Neurosci. *37*, 6342–6358.

70. Swadlow, H.A., and Weyand, T.G. (1987). Corticogeniculate neurons, corticotectal neurons, and suspected interneurons in visual cortex of awake rabbits: receptive-field properties, axonal properties, and effects of EEG arousal. J. Neurophysiol. *57*, 977–1001.

71. Zhou, Y., Liu, B.H., Wu, G.K., Kim, Y.J., Xiao, Z., Tao, H.W., and Zhang, L.I. (2010). Preceding inhibition silences layer 6 neurons in auditory cortex. Neuron *65*, 706–717.

72. Douglas, R.J., and Martin, K.A. (1991). A functional microcircuit for cat visual cortex. J. Physiol. *440*, 735–769.

73. Cruikshank, S.J., Lewis, T.J., and Connors, B.W. (2007). Synaptic basis for intense thalamocortical activation of feedforward inhibitory cells in neocortex. Nat. Neurosci. *10*, 462–468.

74. Bortone, D.S., Olsen, S.R., and Scanziani, M. (2014). Translaminar inhibitory cells recruited by layer 6 corticothalamic neurons suppress visual cortex. Neuron *82*, 474–485.

75. Harris, K.D., and Thiele, A. (2011). Cortical state and attention. Nat. Rev. Neurosci. *12*, 509–523.

76. Zagha, E., and McCormick, D.A. (2014). Neural control of brain state. Curr. Opin. Neurobiol. *29*, 178–186.

77. Radnikow, G., and Feldmeyer, D. (2018). Layer- and cell type-specific modulation of excitatory neuronal activity in the neocortex. Front. Neuroanat. *12*, 1.

78. Kalmbach, A., Hedrick, T., and Waters, J. (2012). Selective optogenetic stimulation of cholinergic axons in neocortex. J. Neurophysiol. *107*, 2008–2019.

79. Sundberg, S.C., Lindström, S.H., Sanchez, G.M., and Granseth, B. (2018). Cre-expressing neurons in visual cortex of Ntsr1-Cre GN220 mice are corticothalamic and are depolarized by acetylcholine. J. Comp. Neurol. *526*, 120–132.

80. Hay, Y.A., Andjelic, S., Badr, S., and Lambolez, B. (2015). Orexin-dependent activation of layer VIb enhances cortical network activity and integration of non-specific thalamocortical inputs. Brain Struct. Funct. *220*, 3497–3512.

81. Adesnik, H., Bruns, W., Taniguchi, H., Huang, Z.J., and Scanziani, M. (2012). A neural circuit for spatial summation in visual cortex. Nature *490*, 226–231.

82. Haider, B., Häusser, M., and Carandini, M. (2013). Inhibition dominates sensory responses in the awake cortex. Nature *493*, 97–100.

83. Kwan, A.C., and Dan, Y. (2012). Dissection of cortical microcircuits by single-neuron stimulation in vivo. Curr. Biol. *22*, 1459–1467.

84. Yuste, R. (2015). From the neuron doctrine to neural networks. Nat. Rev. Neurosci. *16*, 487–497.

85. Harvey, C.D., Coen, P., and Tank, D.W. (2012). Choice-specific sequences in parietal cortex during a virtual-navigation decision task. Nature *484*, 62–68.

86. Reimer, J., McGinley, M.J., Liu, Y., Rodenkirch, C., Wang, Q., McCormick, D.A., and Tolias, A.S. (2016). Pupil fluctuations track rapid changes in adrenergic and cholinergic activity in cortex. Nat. Commun. *7*, 13289.

87. Larsen, R.S., and Waters, J. (2018). Neuromodulatory correlates of pupil dilation. Front. Neural Circuits *12*, 21.

88. Busse, L., Cardin, J.A., Chiappe, M.E., Halassa, M.M., McGinley, M.J., Yamashita, T., and Saleem, A.B. (2017). Sensation during active behaviors. J. Neurosci. *37*, 10826–10834.

89. Zarrinpar, A., and Callaway, E.M. (2006). Local connections to specific types of layer 6 neurons in the rat visual cortex. J. Neurophysiol. *95*, 1751–1761.

90. Bourassa, J., and Deschênes, M. (1995). Corticothalamic projections from the primary visual cortex in rats: a single fiber study using biocytin as an anterograde tracer. Neuroscience *66*, 253–263.

91. Frandolig, J.E., Matney, C.J., Lee, K., Kim, J., Chevée, M., Kim, S.-J., Bickert, A.A., and Brown, S.P. (2019). The synaptic organization of layer 6 circuits reveals inhibition as a major output of a neocortical sublamina. Cell Rep. *28*, 3131–3143.e5.

92. Chen, T.W., Wardill, T.J., Sun, Y., Pulver, S.R., Renninger, S.L., Baohan, A., Schreiter, E.R., Kerr, R.A., Orger, M.B., Jayaraman, V., et al. (2013). Ultrasensitive fluorescent proteins for imaging neuronal activity. Nature *499*, 295–300.

93. Sillito, A.M., Cudeiro, J., and Jones, H.E. (2006). Always returning: feedback and sensory processing in visual cortex and thalamus. Trends Neurosci. *29*, 307–316.

94. Tsumoto, T., and Suda, K. (1980). Three groups of cortico-geniculate neurons and their distribution in binocular and monocular segments of cat striate cortex. J. Comp. Neurol. *193*, 223–236.

Please cite this article in press as: Augustinaite and Kuhn, Complementary Ca^{2+} Activity of Sensory Activated and Suppressed Layer 6 Corticothalamic Neurons Reflects Behavioral State, Current Biology (2020), https://doi.org/10.1016/j.cub.2020.07.069

95. Schindelin, J., Arganda-Carreras, I., Frise, E., Kaynig, V., Longair, M., Pietzsch, T., Preibisch, S., Rueden, C., Saalfeld, S., Schmid, B., et al. (2012). Fiji: an open-source platform for biological-image analysis. Nat. Methods *9*, 676–682.

96. Harrison, T.C., Sigler, A., and Murphy, T.H. (2009). Simple and cost-effective hardware and software for functional brain mapping using intrinsic optical signal imaging. J. Neurosci. Methods *182*, 211–218.

97. Pologruto, T.A., Sabatini, B.L., and Svoboda, K. (2003). ScanImage: flexible software for operating laser scanning microscopes. Biomed. Eng. Online *2*, 13.

98. Pettersen, E.F., Goddard, T.D., Huang, C.C., Couch, G.S., Greenblatt, D.M., Meng, E.C., and Ferrin, T.E. (2004). UCSF Chimera–a visualization system for exploratory research and analysis. J. Comput. Chem. *25*, 1605–1612.

99. Thévenaz, P., Ruttimann, U.E., and Unser, M. (1998). A pyramid approach to subpixel registration based on intensity. IEEE Trans. Image Process. *7*, 27–41.

100. Holtmaat, A., de Paola, V., Wilbrecht, L., Trachtenberg, J.T., Svoboda, K., and Portera-Cailliau, C. (2012). Imaging neocortical neurons through a chronic cranial window. Cold Spring Harb. Protoc. *2012*, 694–701.

Please cite this article in press as: Augustinaite and Kuhn, Complementary Ca^{2+} Activity of Sensory Activated and Suppressed Layer 6 Corticothalamic Neurons Reflects Behavioral State, Current Biology (2020), https://doi.org/10.1016/j.cub.2020.07.069

STAR★METHODS

KEY RESOURCES TABLE

REAGENT or RESOURCE	SOURCE	IDENTIFIER
Bacterial and Virus Strains		
rgAAV.pCAG.Flex.tdTomato	Addgene	28306
AAV9.Syn.Flex.GCaMP6f	Addgene	100833-AAV9
AAV1.hSyn.TurboRFP.WPRE.rBG	Addgene	105552-AAV1
Deposited Data		
Raw and analyzed data	This paper	Upon request from authors
Experimental Models: Organisms/Strains		
Ntsr1-Cre mouse line, (strain B6.FVB(Cg)-Tg(Ntsr1-Cre) GN220Gsat	030648-UCD	Mutant Mouse Regional Resource Center (MMRRC)
Software and Algorithms		
Psykinematix	KyberVision Japan LLC	http://www.kybervision.net/
FIJI	[95]	https://imagej.net/Fiji/Downloads
IO and VSD signal processor plugin for FIJI	[96]	https://murphylab.med.ubc.ca/io-and-vsd-signal-processor/
ScanImage	[97]	https://www.janelia.org/open-science/scanimage
UCSF Chimera	[98]	https://www.cgl.ucsf.edu/chimera/
TurboReg plugin for FIJI	[99]	http://bigwww.epfl.ch/thevenaz/turboreg/

RESOURCE AVAILABILITY

This study did not generate new resources.

Lead Contact

Further information and requests for resources and reagents should be directed to and will be fulfilled by the Lead Contact, Bernd Kuhn (bkuhn@oist.jp).

Materials Availability

This study did not generate new reagents.

Data and Code Availability

The datasets supporting the current study have not been deposited in a public repository because of the large size (10 TB) but are available from the corresponding author on request.

This study did not generate any sophisticated custom computer code or algorithm.

EXPERIMENTAL MODEL AND SUBJECT DETAILS

Animals

All animal experiments were performed in accordance with guidelines approved by the Okinawa Institute of Science and Technology Graduate University Institutional Animal Care and Use Committee (IACUC) in an Association for Assessment and Accreditation of Laboratory Animal Care (AAALAC International) accredited facility.

We used the Ntsr1-Cre mouse line (strain B6.FVB(Cg)-Tg(Ntsr1-Cre) GN220Gsat /Mmucd, stock number 030648-UCD, Mutant Mouse Regional Resource Center, UC Davis) generated by the GENSAT project [51]. In total 13 male mice, 2 - 3 months old at the time of the cranial window surgery, were used for this study.

Before surgery, mice were group housed in a 12 / 12h light /dark cycle. After the surgery, mice were housed individually with unrestricted water and food supply in a temperature – controlled room with 12 / 12h light / dark cycle. Habituation to the setup and most of the recording was performed during the dark cycle. Habituation began a week before the start of imaging sessions (Figure 1A). On the first day, mice were introduced to the cylinder wheel for 10 – 15 min without head fixation. On the second day, mice

Please cite this article in press as: Augustinaite and Kuhn, Complementary Ca^{2+} Activity of Sensory Activated and Suppressed Layer 6 Corticothalamic Neurons Reflects Behavioral State, Current Biology (2020), https://doi.org/10.1016/j.cub.2020.07.069

were head-fixed on the stage with cylindrical treadmill at the 2P setup for 1 h; the time was increased by 0.5 – 1 h on each successive day up to a period of 3 h. From the third day on, the visual stimuli were presented throughout the training session to minimize the stimulus novelty and mimic the recording conditions. Because mice became habituated to handling, head–fixation, and the treadmill, no anesthesia had to be used before, or during the recording.

METHOD DETAILS

Chronic cranial window surgery

Prior to the surgery, a glass coverslip (5 mm diameter,170 μm thickness; WPI) with silicone access port was prepared as described previously [52]. In brief, an ~1 – 1.5 mm diameter hole was drilled using a high-speed dental drill (OS-40, Osada) with a conical shaped stone drill bit (CA1063, Minimo Precision Instruments and Tools). Afterward, the hole was sealed with silicone (Sylgard 184, Dow Corning Corporation).

With minor modifications, the aseptic chronic cranial window surgery was performed following the procedure described previously [52, 100]. Mice were deeply anesthetized throughout the surgery by a mix of ketamine (100 μg / g, ip.) / xylazine (20 μg / g, ip.) or alternatively, mix of Medetomidine (0.3 μg / g, ip.), Midazolam (4 μg / g, ip) and Butorphanol (5 μg / g, ip). Ophthalmic ointment was applied to the eyes for protection and to prevent dehydration. Carprofen (7.5 μg / g body weight, ip) and dexamethasone sodium phosphate (2 μg / g body weight, im. to quadriceps muscle) were administered to reduce immune response and inflammation, while Lidocaine was used for local anesthesia.

After scalp hair removal with a trimmer and hair removal cream, the head was immobilized in a stereotaxic frame. The skin above the skull was opened with a scalpel and connective tissue slightly pushed away from the lambdoid suture using forceps. The area around the circular craniotomy over V1 (center 3.5 mm posterior of bregma, 2.4 mm lateral, diameter ~4 mm) was thinned using a dental drill. For craniotomy, rather than using forceps for bone lifting, we glued a wooden stick (~2 - 3 mm in diameter e.g., wooden part of a Q-tip) vertically to the center of the craniotomy bone with superglue. Once the superglue had set, the stick was gently lifted to separate the skull from the dura.

The glass window with access port was mounted directly onto the dura. The flattened ends of two EEG silver wires (0.4 mm diameter) were inserted between the glass and dura, such that they framed the craniotomy over the occipital lobe on its lateral and medial sides for EEG recordings. The window was then sealed with superglue to the skull. A rectangular aluminum head-plate was positioned over the cranial window and attached by applying dental acrylic using a toothpick. The dental acrylic was used to fill all of the space under and around the head-plate, including the edges of the glass window and exposed skull. Together with retrograde tracer injection, the surgery took about 2 – 3 hours. If the mouse started to show signs of waking, anesthesia was switched to 0.5 – 1% isoflurane. Every hour, saline (10 - 20 μl / g, sc.) was injected to avoid dehydration. If Medetomidine mix anesthesia was used, after the procedure the mouse was administered Atipamezole hydrochloride (0.3 μl / g, ip.) for faster waking. Prior to waking, as well as on the following or the two following days after the surgery, Buprenorphine (0.1 μg / g, sc.) was injected to ease the pain and reduce distress.

AAV injection to label dLGN axonal projections

In one experiment (Figure 1B; Video S1), AAV1.hSyn.TurboRFP.WPRE.rBG (105552-AAV1, Addgene) was injected through the dura into dLGN (2.45 mm posterior of bregma, 2.4 mm lateral, 2.9 mm ventral) after the craniotomy during the cranial window surgery. The sharp tip beveled quartz pipette (1 mm outer diameter, 0.3 mm inner diameter, ~10 - 15 μm tip opening diameter) was tip-filled immediately before injection. After 3 – 5 min of waiting, about 35 nL of viral vector solution was pressure injected per ~3 min and the pipette was retracted after another 5 min wait.

Retrograde tracer injection

The red fluorescent retrograde tracer (FluoSpheres, 0.04 μm, 580 – 605 nm; Invitrogen) was injected through the dura into dLGN (2.45 mm posterior of bregma, 2.4 mm lateral, 2.9 mm ventral) after the craniotomy during the cranial window surgery. A beveled sharp tip quartz pipette (1 mm outer diameter, 0.3 mm inner diameter, beveled to ~20 μm tip opening diameter) was tip-filled with tracer solution (mixed 1:1 with PBS and sonicated immediately before the filling). The pipette with tracer solution was slowly lowered into the brain. After 3 – 5 min of waiting, about 150 - 200 nL of tracer solution was pressure injected over ~10 – 15 min. The pipette was retracted after another 10 min waiting period.

Retrograde AAV injection to sparsely label dLGN-projecting L6CT neurons

In a subset of experiments, instead of fluorescent beads, the viral vector rgAAV.pCAG.Flex.tdTomato (28306, Addgene) was injected into dLGN. The sharp tip beveled quartz pipette (1 mm outer diameter, 0.3 mm inner diameter, ~10 - 15 μm tip opening diameter) was tip-filled immediately before injection. After 3 – 5 min of waiting, about 35 nL of viral vector solution was pressure injected per ~3 min and the pipette was retracted after another 5 min wait.

Viral injection through the port of the cranial window

When the retrograde labeling appeared in cortex (7 – 14 days), a viral vector AAV9.Syn.Flex.GCaMP6f (100833-AAV9, Addgene) was injected through the silicon port of the cranial window to infect L6 neurons already labeled with retrograde tracer. With minor modifications, the injection through the access port was performed following the procedure described previously [52]. Mice were deeply

anesthetized with 1% isoflurane and head-fixed on the microscope stage. Anesthesia was maintained throughout the whole procedure. Once the intended injection area has been identified using 2P imaging (25 × /1.05, Olympus), the pipette trajectory estimation and injection was done with brightfield imaging using a low magnification and long working distance objective (2.5 × /0.12, Zeiss). This was necessary since a relatively steep angular trajectory (37 – 39°) was needed for the pipette to reach the dorsally and 0.95 – 1 mm deep injection area through the access port. A beveled sharp tip quartz pipette (1 mm outer diameter, 0.3 mm inner diameter, ~10 μm tip opening diameter) was tip-filled with viral vector solution and mounted on a micromanipulator. The pipette movements were controlled with a micromanipulator (MP-285, Sutter Instruments) under visual guidance to avoid blood vessels. Usually, 70 – 100 nL of solution was pressure injected during 5 – 10 min into each of 2 - 3 injection sites, located 150 – 300 μm apart, but within the L6 area densely labeled with retrograde tracer. Waiting periods of 3 – 5 min and 5 – 10 min preceded every injection and pipette retraction, respectively.

Intravitreal TTX injection

After 2P imaging sessions to collect control data, mice were removed from the stage, deeply anesthetized with 3% isoflurane and positioned on their side under a wide-field microscope. Anesthesia (1% isoflurane) was maintained throughout the procedure. The area around the eye was pressed slightly to expose the temporal side of the eyeball. A sterile 26 -gauge needle was used to puncture sclera just below limbus. Then, tetrodotoxin (TTX, 1 μl, 1mM in saline, Sigma) was injected into the vitreous chamber using a micro syringe (Hamilton). Mice were again head-fixed on the imaging stage 1.5 – 2 h after the TTX injection. Retinal inactivation (both eyes) was verified by the dilated pupil and the absence of pupillary light reflexes. The imaging experiment was repeated at the same imaging site as the control, so that the activity of the same neurons could be compared.

Ophthalmic application of Atropine

After control 2P imaging sessions, mice were lightly anesthetized with 1% isoflurane without removing them from the stage. Then, atropine sulfate (Atropine, 100 μl drop of 1% in PBS, Nacalai tesque) was applied on both eyes. Atropine dilated the pupil and abolished pupillary light response within ~5 min and no signs of relief were observed within the following 24 h. The imaging session resumed after the mouse recovery to normal behavior (30 min in the darkness). The imaging experiment was repeated at the same imaging site as the control, so that the activity of the same neurons could be compared.

Visual stimulation

Visual stimuli were generated in Psykinematix (KyberVision Japan LLC) and displayed on an LCD monitor (Dell 47.5 × 26.5 cm, 60 Hz refresh rate, gamma corrected with a Konica Minolta LS-150 luminescence meter) positioned at a 45° angle to the mouse axis, 15 cm from the eye on the contralateral side of the imaging window. Full-field drifting gratings (RGB black (luminance 0.16 cd m^{-2}) / blue (luminance 12.6 cd m^{-2}; mean luminance 6.51 cd m^{-2}) were used during two photon and intrinsic signal imaging. For intrinsic signal imaging four direction (135°, 180°, 225° and 270°; temporal frequency 2 Hz, spatial frequency 0.1 cycles per degree) drifting gratings were presented (250 ms each angle, total stimulus length 1 s). The core experiments were made using eight different directions (step 45°, temporal frequency 2 Hz, spatial frequency 0.08 cycles per degree). The gratings were presented in a pseudo – random order during two photon imaging. The duration of the visual stimulus was 2 s and the intertrial interval (black, mean luminance 0.16 cd m^{-2}) was 12 s. In a sub-set of experiments (Figure 6D) stimulus on- was 5 s and off- was 15 s. A second set of visual stimuli (Figure 6E) consisted of 10 full screen drifting gratings: 2 movement directions (0° and 270°) at 5 spatial frequencies (0.01, 0.02, 0.04, 0.06 and 0.1 cycles/deg), 2 Hz speed, presented for 4 s with 14 s inter-trial intervals (or for 6 s with 20 s inter-trial intervals). A third set of stimuli (Figure 6F) consisted of 3 different full screen illumination intensities (RGB blue/black: 100, 50 and 25%; luminance, corresponding to 12.6, 6.5 and 3.2 cd m^{-2}) full-field presentation for 5 s with 20 s inter-trial intervals or for 7.5 s with 30 s of inter-trials.

Intrinsic signal imaging

To reveal the location of the intended V1 imaging site, we used intrinsic signal imaging (Figure 1A). Mice were deeply anesthetized throughout the imaging procedure by a mixture of ketamine (100 μg / g, ip.) / xylazine (20 μg / g, ip.) or alternatively, mix of Medetomidine (0.3 μg / g, ip.), Midazolam (4 μg / g, ip) and Butorphanol (5 μg / g, ip) supplemented with 0.25 – 0.75% isoflurane in O_2 when head fixed on the microscope stage. Such a combination was necessary to immobilize the eyeball and keep the pupil slightly dilated and stable. Isoflurane would dilate the pupil and maintain the stable level of anesthesia. Without ketamine / xylazine (or mix of Medetomidine), however, intrinsic imaging would often fail because of spontaneous changes in pupil diameter and rolling of the eyeball. The body temperature (36 - 37°C) was maintained during imaging with a feedback-regulated heating pad (FHC 40-90-8D). In the case of Medetomidine mix anesthesia, immediately after the procedure, the mouse was administered Atipamezole hydrochloride (0.3 μl / g, ip.) for faster waking.

For intrinsic signal imaging, the cortex was illuminated with a high-power red LED light source (RLX 615-655 nm, X-Cite XLED1). Images (1200 × 925 pixel frames, corresponding to 4.025 × 3.14 mm) were taken by a sCMOS camera (PCO.edge, PCO) through the custom-built microscope (MOM, Sutter Instruments) and an objective (5 × /NA0.2, Zeiss) focused 400 - 600 μm below the cortical surface. The 5 s recording (193 frames / s) consisted of 1 s black screen, 1 s visual stimulation, and 3 s black screen (see Visual stimulation in Experimental procedures for details). The recording was repeated 9 – 20 times with a 2 min black screen (mean luminance 0.16 cd m^{-2}) intertrial interval.

Please cite this article in press as: Augustinaite and Kuhn, Complementary Ca^{2+} Activity of Sensory Activated and Suppressed Layer 6 Corticothalamic Neurons Reflects Behavioral State, Current Biology (2020), https://doi.org/10.1016/j.cub.2020.07.069

Recorded stacks of images were processed using FIJI (US NIH [95]) plugin "IO and VSD signal processor" [96]. The average ratio image, showing stimulation induced changes in red light reflectance, was calculated from averages of baseline images (before stimulation) and averages of response images. The average ratio image was adjusted to a threshold for the color map, to project the functional area of V1 on the cortical surface. The threshold was based on 50% of the maximal peak measured from the smoothed intensity histogram (moving average of 10 points) made of manually drawn ROI of the functional area of V1 (Figure 1A).

Two photon calcium imaging and behavioral state recording

After 7 days of habituation to the experimental setup, 3 – 4 weeks after viral injection, 2P calcium imaging experiments were started. Imaging of one plane was conducted for typically 1 - 3 h / day. If necessary, the imaging of the same neurons was repeated in the following days to collect activity during additional behavioral states or under different experimental conditions. The same imaging plane was found using images of the superficial blood vessel pattern (e.g., Figure 1A) and neuronal somas (e.g., Figures 1C and S1B). The dataset of 1-2 h (73 ± 18 min) / 2-4 (3 ± 1) days per mouse (n = 3) was used for the core of this study.

Imaging was performed using a custom-built 2P microscopes with either resonant or galvo- scanning systems (MOM, Sutter Instruments) with a water immersion objective (25 × /1.05, Olympus). Brightfield imaging (for blood vessel pattern) was done with an air objective (5 × /0.2, Zeiss) and sCMOS camera (PCO.edge, PCO) in the green spectral range (470 – 575 nm; Chroma). The fluorescence was excited using an ultrafast Ti:sapphire laser (950 nm; Vision II, Coherent) and detected with two GaAsP photomultiplier tubes (Hamamatsu) in the green (490 - 560 nm) and red (570 - 640) spectral range using corresponding filters separated by a 565-nm dichroic mirror (all Chroma).

The data for reconstruction of L6 neurons (e.g., Figures 1B and 7A and Video S1: Z axis from dura to 800 – 900 μm below, 0.5 Hz frame rate, 5 - 9 averages, Z step 2 μm, 512 × 512 pixel corresponding to 500 × 500 μm^2 field of view with 25 × objective) was collected using ScanImage [97] on a 2P microscope with galvo scanners (MOM, Sutter Instruments).

A 2P microscope with resonant scanning system (MOM, Sutter Instruments) was used for functional calcium imaging. The point spread function of excitation was extended by under-filling of the objective back aperture and adjusting the objective collar to maximal imaging depth [56]. Thereby, the point spread function was extended to 1 μm x 1 μm x 5 μm. The laser power was kept in the range of 50 – 75 mW to record in upper (500 – 675 μm cortical depth; 602 ± 59 μm, n = 7) as well as deeper (down to about 780 μm, n = 2) L6. Images were acquired at 30.9 Hz at a resolution of 512 × 512 pixel corresponding to a 400 × 400 μm^2 field of view with the 25 × objective (NA. 1.05, Olympus). The microscope setup and data acquisition were controlled by commercial software (MScan, Sutter Instruments).

Synchronized with 2P imaging data, MScan recorded a behavior movie and analog signals (1 kHz) of (a) timing of image acquisition (i.e., command signal to scanners), (b) EEG, (c) treadmill motion, and (d) visual stimulation on/off triggers. The behavior movie (30.9 frames / s, synchronous with 2P images) was recorded under constant infrared illumination (LED M850L3, Thorlabs) using a CCD camera (CSFV90BC3, Toshiba Teli) with macro lens (Nikkor 50mm f/1.2; Nikon) positioned at a distance of 15 cm from the eye on the ipsilateral side of the imaging window. The pupil was bright due to scattered light of the infrared 2P excitation laser beam. The electroencephalogram was recorded using an EEG preamplifier (100 × gain; Sigmann Elektronik) with additional amplification (2.4 × gain; Model 440, Brownlee Precision) and band-pass filtering (0.25 – 100 Hz; Model 440, Brownlee precision). The treadmill rotation was measured using a rotary encoder (E6A2, Omron) with 1 degree angular resolution.

QUANTIFICATION AND STATISTICAL ANALYSIS

Offline data analysis was performed with FIJI (NIH [95], MATLAB (MathWorks), Igor Pro (WaveMetrics), UCSF Chimera (NIH [98],) and SPSS Statistics (IBM). Results are given as mean ± sd unless indicated otherwise.

Ca^{2+} imaging analysis

First, movies (30.9 Hz) of GCaMP6f fluorescence changes were smoothed using 3D Gaussian filter (X, Y and Z sigma = 1, FIJI). Then, a template image was created by average intensity Z projection of a few seconds of the movie, when the mouse was sitting still, and no motion artifacts could be detected by manual inspection. This template was used for motion artifact correction with the FIJI plugin "TurboReg" [99] for all recordings acquired in that particular imaging plane. Regions-of-interest (ROIs) for all putative cell somata and major dendritic processes where then selected manually (Figure S1C). Overlapping ROIs areas where subtracted and only residual ROIs of somas larger than 64 pixels were used for Ca signal extraction. After excluding overlapping regions, signals of neighboring ROIs showed no cross talk and no contamination by neuropil signals (Figures S1D and S1E). The time trace of each cell (e.g., Figure S1E) was calculated as the averaged pixel intensity of the residual ROI.

Light artifacts caused by the visual stimuli were corrected by subtracting the averaged time trace of a dark ROI (blood vessel). The $(\Delta F/F)(t)$ was calculated as $(F(t) - F_B(t)/F_B(t))$, where baseline $F_B(t)$ was calculated as a line interpolating the intensities at the beginning (first quartile of the intensity values of the first 2 – 4 min) and the end (first quartile of the last 2 – 4 min) of the recording session. In rare cases, typically among VSS neurons, automated baseline correction would fail because of the high neuronal activity at the specified intervals. Therefore, each neuronal trace was inspected manually. In case of the failure, the baseline correction would be done by selecting individual 2 – 4 min periods of low or no activity periods.

LGN projecting corticothalamic neurons (CT), i.e., neurons with clear co-localized calcium indicator and retrograde tracer (beads or retro-tdTomato) were selected manually, using full ROIs in the superimposed red / green image of the imaging plane (Figure 1C) and

Please cite this article in press as: Augustinaite and Kuhn, Complementary Ca^{2+} Activity of Sensory Activated and Suppressed Layer 6 Corticothalamic Neurons Reflects Behavioral State, Current Biology (2020), https://doi.org/10.1016/j.cub.2020.07.069

superimposed red / green stack of images of L6. About 60% of GCaMP6f expressing neurons had fluorescent microbeads (485 out of 820, 59 ± 7%, 3 mice), therefore were specified as corticothalamic and used as core dataset in this study. About 70% of tdTomato expressing neurons had functional GCaMP6f signals (87 out of 123, 69 ± 7%, 2 mice). The apical dendritic processes of about 40% of these neurons could be traced up within the cortical volume stack and were reconstructed using UCSF Chimera (33 out of 87, 37 ± 4%, 2 mice; Figures 7A–7D).

Behavioral state characterization and data sorting

The EEG (recorded at 1 kHz) was bandpass filtered (0.25 Hz – 100 Hz range) and power spectra calculated using Fast Fourier Transformation (FFT, 4 s segments (step 1 s), 0.25 Hz resolution). The EEG delta (1 – 4 Hz) power (%) was calculated by normalizing to the maximal delta power of all recordings from each mouse.

Pupil size (or exposed pupil area) was extracted after binarizing the behavior movie around the eye (FIJI). The pupil size (%) was calculated by normalizing to the maximum pupil size of all movies for each mouse. To eliminate pupillary reflex-caused changes of the size during the visual stimulation, the new trace (pre-stimulus pupil size) was constructed using the pupil size in the darkness only, by interpolating between consecutive pupil sizes averaged during 1 s before the visual stimulus presentations.

Data from episodes of rapid-eye movement (REM) sleep (defined as periods of a low EEG delta power, but small pupil size), grooming (intensity was defined as variance of the average pixel intensity values within the ROI of a snout from the behavior movie) and blinking (pupil size = 0%) were removed from the analysis.

The Ca^{2+} signal, EEG, pupil size and locomotion speed traces were divided into visual stimulation trials (12 s duration) with timing aligned to the onset of the stimulus: 5 s before, 2 s on- and 5 s after offset. Each trial was ranked according to 5 behavioral state levels, which were defined using locomotion and the pre-stimulus pupil size. State 1 (BS1) trials were defined as trials when the mouse was moving with an average treadmill speed above 1 cm/s for 3 s before – 2 s during – 3 s after the visual stimulus presentation. BS2 - BS5 trials were defined as trials, when the mouse was stationary: an average treadmill speed below 0.5 cm/s for 3 s before – 2 s during – 3 s after the visual stimulus presentation. The pupil (average size during 1 s before visual stimulus onset) was largest for the most alert BS2 trials (> 70%) and smaller for less alert and more sleepy trials: BS3 (from 70 to 30%), BS4 (from 30 to 10%) and BS5 ($\leq$10%).

Spontaneous calcium activity was calculated as average $\Delta F/F$ of 4 s before the stimulus onset while visually evoked activity was calculated as average $\Delta F/F$ of 4 s after the onset of the visual stimulus. The neuronal response was calculated as baseline activity (average $\Delta F/F$ of 2 s before the stimulus onset) subtracted from visually evoked activity (average $\Delta F/F$ during stimulus onset + 2 s after offset).

To test how CT neuronal activity relates to behavioral state reflecting parameters, we calculated correlations (Spearman correlation coefficient *rho* (ρ, Figure 3) between the calcium signal ($\Delta F/F$; 4 s time periods before the onset of visual stimulation for visual stimulus suppressed (VSS) neurons, and 4 s time periods after for visual stimulus activated (VSA) neurons) and locomotion speed as well as pupil size. Additionally, using the pupil size trace, the state-change trials (Figure 5C) were defined as 100 s periods aligned to an average of pupil size baseline of $\leq$ 30% (10 s before the onset of visual stimulus) followed by an increase in pupil size to $\geq$ 50% within 50 s after the onset of the following visual stimulus (n = 52 trials; 26, 11 and 15 trials from 3 mice). Only episodes when the mouse was stationary, were used to estimate neuronal activity correlation with pupil size or neuronal activity change during the state shift, to separate locomotion and state change effects.